9. Measurements of the discharge current.

Although the main thrust of the present experimental work has been towards the direct measurement of concentrations of metastable atoms by optical absorption, some attention was also paid to measurements of the current passed by the pre-breakdown discharge. There are several reasons for this. Firstly, some of the discharge parameters yielded by the optical method may be determined independently by measurements of the discharge current. Measurements of current under these circumstances act as a check against possible systematic errors in the optical method. Secondly, there are some parameters, such as γ_i, the efficiency of secondary ejection by ions, which are not easy to determine from optical measurements of the metastable concentration. The occurrence of damped sinusoid terms in the decay of slow current, which is predicted by the theory described in chapter 3 section 2, is also best investigated by measurements of current alone. Lastly, it is of interest to compare values of the primary ionisation coefficient α_i derived by using time-resolved measurements of discharge current with those of previous workers. As is described in section 9.1, previous measurements of α_i in argon have been made almost exclusively by measurements of the total steady-state current, allowing for the possibility of error due to the variation with electrode separation d of the generalised secondary coefficient $\overline{\omega}(d)/\alpha_i$ (see section 2.2.3).

9.1. Measurements of the primary and secondary ionisation coefficients.

There have been a large number of experimental determinations of the primary ionisation coefficient α_i in argon. A comprehensive list of those performed prior to 1973 may be found in Dutton (1975); subsequent to this date, Lakshminarasimha and Lucas (1977), Abdulla *et al* (1979), Burgmans and Smeets (1983) and Dall'Armi *et al* (1992) have also measured the quantity. A representative sample of four sets of measurements is displayed in figure 9.1.

The most extensive and precise set of measurements appears to be that of Kruithof & Penning (1936), extended and summarised by Kruithof (1940). These authors used the basic Townsend technique, in which the steady-state current passed by the discharge is measured at several values of the electrode separation d, the potential difference being varied in proportion to d so that the electric field remains constant. The constancy of the electric field ensures that the average energy of the electron stream remains the same at all

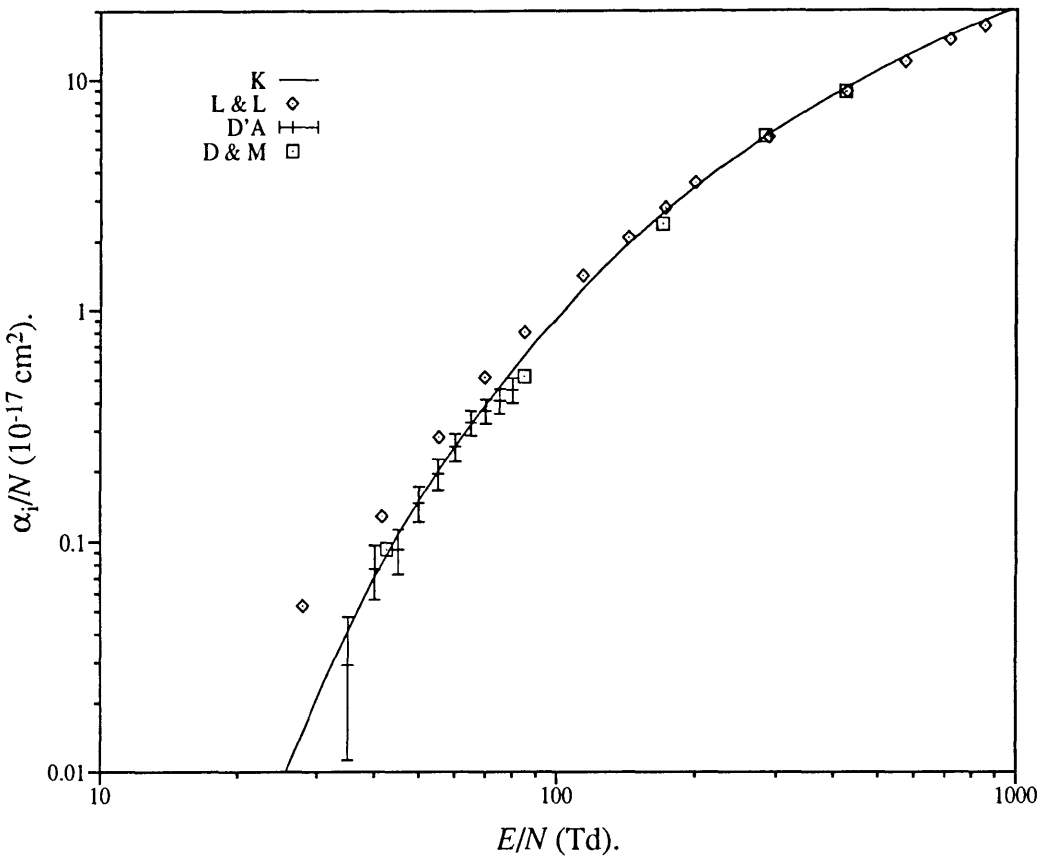

Figure 9.1. Previously reported measurements of α_i/N (the reduced primary ionisation coefficient) for argon. In the legend, "K" refers to the data of Kruithof (1940), "L & L" to Lakshminarasimha and Lucas (1977), "D'A" to Dall'Armi *et al* (1992) and "D & M" to Davies and Milne (1959).

times. The increase in current is then given by equation (2.9). Kruithof and Penning used a three-point method to analyse their data, which is the most economic in terms of the number of measurements which need to be made, but which yields much less precise results than the Gosseries method, in which many more data values may be used. Despite this, the data of Kruithof and Penning exhibit a remarkably low degree of scatter.

Kruithof and Penning were not able to take into account the contribution of metastable excited argon atoms. These authors paid considerable attention to the purity of the gas samples used. The vacuum was maintained by a mercury diffusion pump, with liquid air traps to prevent contamination of the samples by mercury vapour. No base pressure is quoted but, after briefly heating the chamber as a whole to 470 °C and the cathode to red heat, the increase in pressure was 2.5×10^{-4} Torr in 24 hours, a rate

comparable with that in the present apparatus. It seems almost certain, therefore, that sizeable metastable concentrations would have been present in the argon discharges of Kruithof and Penning. If a significant proportion of the secondary ionisation is caused by the ejection of electrons from the cathode by metastable impact, the generalised secondary coefficient $\overline{\omega}(d)$ is likely to be a function of the electrode separation, for reasons described in chapter 2. This may distort the value of α_i obtained from measurements of the steady-state current. Evidence for just such a perturbation by the effect of metastables can be found in similar experiments performed with neon, krypton and xenon. In these gases, the values of α_i determined by Kruithof and Penning (1937) and Kruithof (1940), as well as those of subsequent workers using the same Townsend method, were not confirmed by measurements made using the 'luminous flux' method (see Buursen *et al* 1972, Bhattacharya 1976 and Jacques *et al* 1986): the 'luminous flux' values of α_i were found to be lower than the 'Townsend' values for all the above-mentioned gases. This is to be expected, since the 'luminous flux' technique allows the direct measurement of the exponential increase in electron concentration across the discharge gap and ought, therefore, to be immune from the influence of metastable atoms. More recently, Brunker (1984) was able to subtract the contribution made by metastable atoms to the ionisation in pre-breakdown neon by performing time-resolved measurements of the discharge current (see chapter 3, section 3.2 for a description of this technique, first applied by Haydon and Williams (1976) to the nitrogen discharge). Brunker derived values of α_i in neon which are consistent with those of Buursen *et al* rather than those of Kruithof and Penning. On the other hand, Dutton (1981) has pointed out that luminous flux measurements have usually been performed in self-sustained discharges, which, in order to increase the light output, run at much higher currents than is usual in the pre-breakdown regime. In such discharges, the current is spread across the whole of the cathode (see the breakdown limit curve on figure 6.3, for example); the effect of the non-equilibrium fields at the electrode edges must therefore be considered. Space charging could also be a problem. In these circumstances, it is not certain that correct values of α_i can be determined.

Unfortunately, no 'luminous flux' measurements appear to have been performed in pure argon. There is therefore little independent evidence that Kruithof and Penning's determination of α_i in argon is in error. There appears to be only one other study in which the contribution made by metastable atoms was specifically excluded, this being the experiment of Dall'Armi *et al* (1992). These authors employed a pulsed excitation, which allowed the contributions made by various species to be separated in time. As can be seen

from figure 9.1, their values appear to be trending below the line of Kruithof's results at high *E/N*, although the difference is barely significant.

Impurities in the gas used may be efficient quenchers of metastable activity (see, for example, the data of Velazco *et al* (1978) concerning the common impurities H_2O, CO, H_2, N_2, O_2). Measurements performed (without subtracting the metastable contribution) in impure gas might, therefore, be expected to result in values of α_i below those which were obtained in pure gas. However, the reverse is true: see, for example, the results of Heylen (1968a), Lakshminarasimha and Lucas (1977) and Abdulla *et al* (1979). This has been attributed to Penning ionisation of impurity particles by argon metastables. Indeed, measurements of the ionisation coefficient α_i in argon which has been intentionally contaminated with Penning-ionisable gases such as Hg (Burgmans and Smeets 1983) and certain volatile hydrocarbons (Heylen 1968a, b) confirm that a Penning contribution does inflate the effective value of α_i. However, every one of the impurity species named at the start of the paragraph, together with other possible contaminants such as Ne, Kr, Xe, OH, H, O and N, has an ionisation energy which is too high for the molecule to be Penning-ionisable by argon $1s_3$ or $1s_5$ metastables. There seem to be two reasonable conclusions to be drawn. The first is that the Penning-ionised contaminants reported by both Heylen (1968a) and Abdulla *et al* (1979) were hydrocarbons of low molecular mass rather than the more electronegative gases listed above. The other is that another, more energetic metastable state exists in the discharge. There are no other metastable states of the neutral argon atom, but the potential curves of the dimer are very poorly explored, and it is possible that additional long-lived, energetic states of this molecule may exist (the known metastable dimer states do not have enough energy). Any such state would need to have a lifetime of several μsec (Melton *et al* 1954), which is consistent with the radiative lifetimes of other metastable Ar_2 states (Boucique and Mortier 1970, Moutard *et al* 1987).

The second conclusion is supported both by the results obtained by Heylen in argon which had been intentionally mixed with a small quantity of methane, which is not Penning-ionisable by argon 1s states, and also by the experiments of Bertolini *et al* (1953) and Melton *et al* (1954), in which an increase was observed in the ionisation produced by alpha particles in argon when the gas was mixed with small amounts of impurity. Most of the gases listed above were tried, with positive results in nearly all cases.

It was decided to employ the technique of Haydon and Williams (1976) to measure the variation of α_i with *E/N* in argon. The procedure is the same as for the Molnar

experiment, which is essentially the Townsend experiment with a chopped source of primary current. At a selection of values of *E/N*, measurements are taken at a number of electrode separations while the electric field is maintained at a constant value. The discharge is turned on and off by a square-wave modulation of the intensity of the ultraviolet lamp which is the source of the primary current. As described in section 3.2, time-resolved detection of the resulting discharge current allows the contribution made by metastable-produced secondaries to be subtracted from the total steady-state current. In the present experiment, this was done by fitting functions to the decay of current after the lamp was switched off. A straight line was fitted by standard linear regression to the 'pedestal' of the signal, ie that part of the signal which occurs before the lamp switch-off time; a function consisting of a sum of two exponentials was fitted to the slow current decay, using the techniques described in section 8.3. The amplitudes of the exponentials were subtracted from the pedestal height to yield the amplitude of the fast current decay. These amplitudes were then analysed by the Gosseries technique (Gosseries 1939; cf. chapter 2, section 2.1). A fairly well-behaved example of such a plot is shown in figure 9.2.

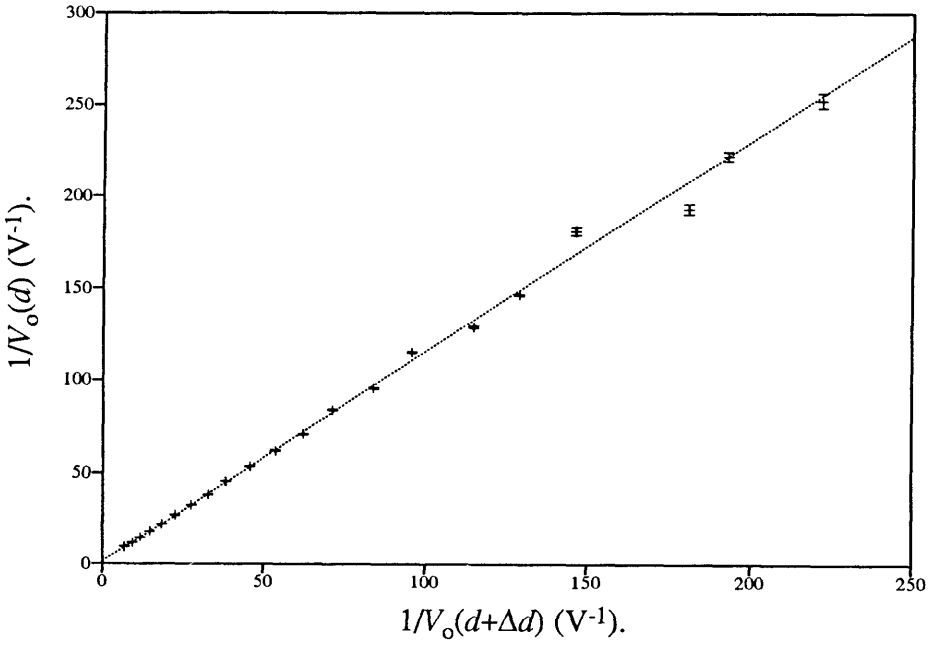

Figure 9.2. A Gosseries plot of discharge current data taken at a pressure of 3 Torr and a reduced electric field of 50 V cm^{-1} Torr^{-1}. The currents were detected using the scheme described in chapter 7. The data values are given in terms of $V_0(d)$, the voltage recorded at the output of the Tektronix amplifier as a function of the electrode separation d. The dotted line was fitted by linear regression, with the data points weighted in inverse proportion to their y-coordinate uncertainties (Weisberg 1980). The x-coordinate uncertainties are of similar size to the y, but are not shown on the figure.

No curvature of these plots could be detected, such as has been reported in hydrogen by Folkard and Haydon (1971a, b); however, the data points were frequently scattered more widely than their individual uncertainties might lead one to expect. It appears therefore that the uncertainty estimates generated by the fitting procedure may be too small. Further evidence for this is presented in the next section.

Measurements were made of α_i at several different pressures, for a selection of values of the reduced electric field *E/N*. The results, which are displayed in figures 9.3, 9.4 and 9.5, confirm that α_i is proportional to the gas number density *N*.

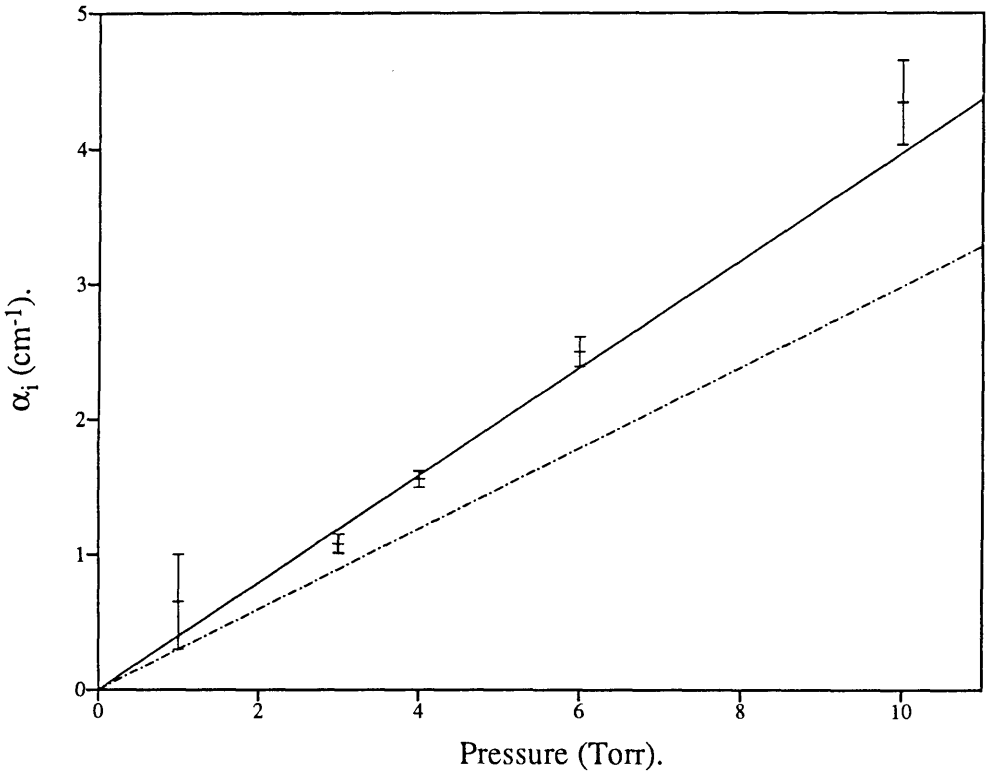

Figure 9.3. Values of the primary ionisation coefficient α_i recorded at various pressures. These values were measured at a reduced electric field *E/p* of 33.3 V cm^{-1} Torr^{-1} at 300 K. The solid line was fitted to these data points using a weighted-least-squares routine (Weisberg 1980); the slope of the chained line is equal to the value of α_i/p measured by Kruithof (1940) at this value of *E/p*.

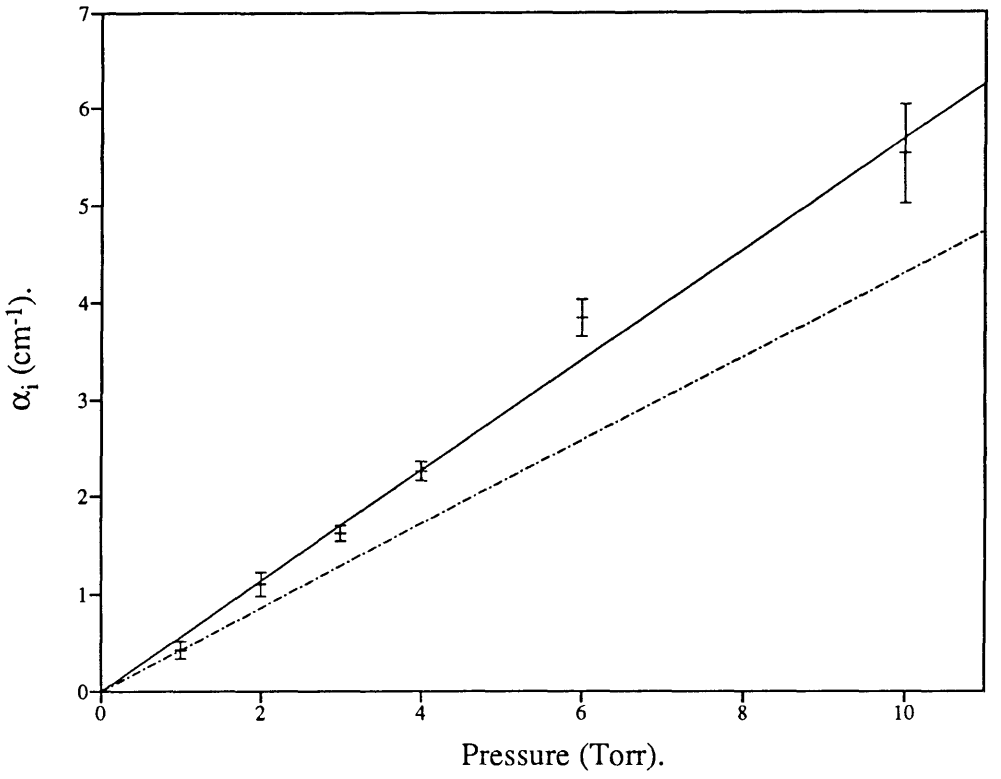

Figure 9.4. Same as figure 9.3, except *E/N* is here equal to 40 V cm^{-1} Torr^{-1} at 300 K.

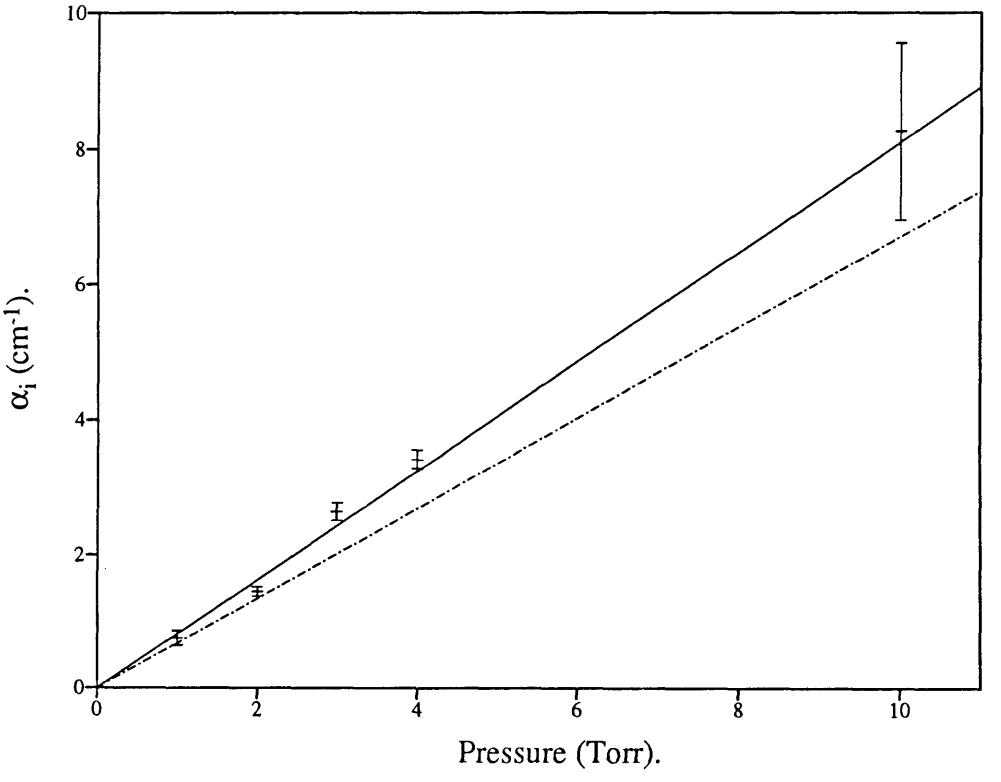

Figure 9.5. Same as figure 9.3, except *E/N* is here equal to 50 V cm^{-1} Torr^{-1} at 300 K.

The results of these experiments are displayed in figure 9.6, with Kruithof's 1940 data set included for comparison.

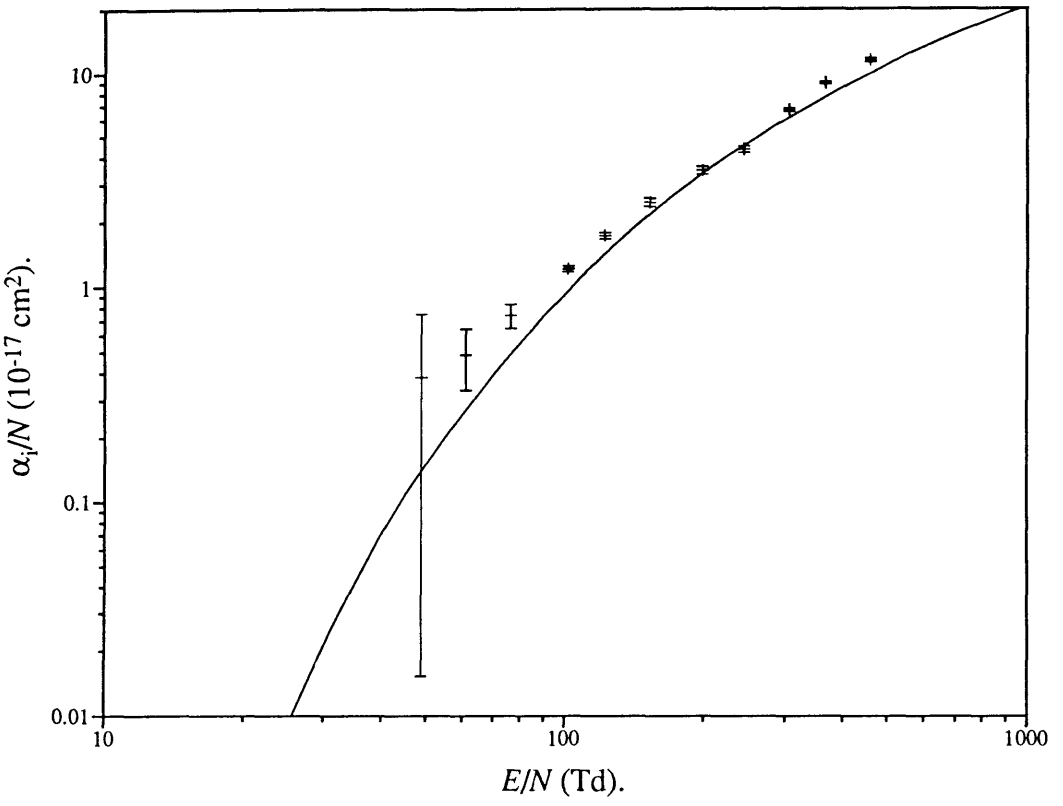

Figure 9.6. Values of α_i/N determined in the present study (error bars), compared to the data of Kruithof (1940) (solid line).

It is interesting to note that the present values are *larger* than Kruithof's at almost all values of *E/N* that were examined. Indeed, the present values follow the trend of Lakshminarasimha and Lucas' data rather closely below 300 Td. This is perhaps a little surprising. Although the purity achieved in the present apparatus was less than optimum, the system was considerably cleaner than that of Lakshminarasimha and Lucas. These authors were not overly concerned with the purity of the gases used, since their primary interest was the measurement of electron diffusion coefficients, which are relatively insensitive to trace contaminants. They report no heat treatment of their vacuum system (the apparatus is described fully in Virr *et al* 1972), which was evacuated by an oil

diffusion pump, with liquid air traps. The base pressure they obtained was about 1×10^{-6} Torr, more than 30 times higher than that achieved in the present apparatus.

An attempt was made to compare the above results with a set made using the unmodified Townsend method. In order to measure the steady-state current, the amplifier, DSO and computer interface were replaced by an electrometer, as described in section 7.2.1. It was found to be very difficult to perform reliable measurements, due to the outgassing of impurities mentioned in section 7.1. The resulting steady increase in the quenching rate had a marked effect on the total discharge current, particularly in the approach to breakdown. Only two sets of these measurements are thought to be reliable. These were performed immediately after the first getter was applied (see chapter 7, section 7.1), which reduced the outgassing rate to a negligible level for a short period. These measurements, performed respectively at values of *E/N* of 312 and 379 Td (ie, 100 and 120 V cm^{-1} Torr^{-1}) returned values of α_i which were not significantly different from the values shown in figure 9.6.

As described in chapter 2, the *y*-intercept of the Gosseries plot is equal to the secondary ionisation coefficient γ_i divided by I_0, the discharge current in the limit of $d \to d_0$. If I_0 is known, the value of γ_i can therefore be deduced. Unfortunately, I_0 was difficult to measure with accuracy using the time-varying technique. In principle the value ought to be identical to that measured by recording the steady-state current, since the ratio I_{fast}/I_{total} (see figure 3.4 on page 37) becomes close to 1 at small values of *d*. However, this was not found to be the case, possibly because the nominal value of the load resistance used for steady-state measurements was incorrect.* In any case, it was necessary to find some alternative way of measuring γ_i. As described in chapter 2, at the end of section 1, a plot of $\exp[\alpha_i(d-d_0)]/I(d)$ against $\exp[\alpha_i(d-d_0)]-1$ allows the quantity to be determined. An example appears in figure 9.7.

*This resistance is usually much larger than that used in the time-dependent method, 10^{10} ohms being a typical value. Because resistances of this size are difficult to measure, the nominal values were not independently confirmed.

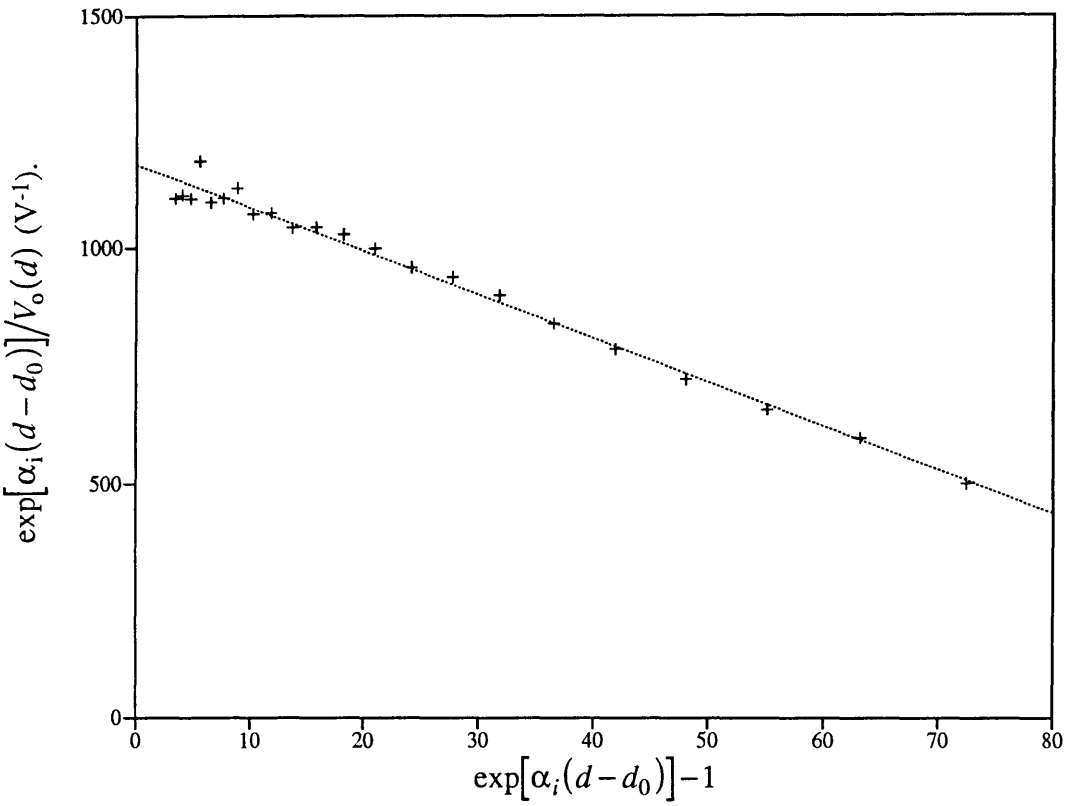

Figure 9.7. A plot of the type described in chapter 2, section 2.1. The slope is proportional to $\gamma_i/V_0(0)$ and the intercept to $1/V_0(0)$. The voltage $V_0(d)$ is given by $V_0(d) = gR_L I(d)$, where R_L is the load resistance, g is the amplifier gain and $I(d)$ is the current passed by the discharge at an electrode separation d. The dotted line, which was fitted to the data points using a straightforward linear regression, gives a value of 0.79% ± 0.02% for the secondary coefficient γ_i.

Time did not permit an exhaustive examination of the reliability of this type of plot. Two observations were made that have a bearing on this, however. Firstly, it was noticed that a poor choice of α_i often resulted in the points lying on a curve rather than a straight line. Of course, the reverse, that a straight plot implies a reliable value of α_i, is not necessarily true. Secondly, the scatter in the points was much greater than the uncertainties in the individual points. For example, the uncertainties in the individual data points of figure 9.7 are too small to be detectable on the scale of this plot. The phenomenon can also be detected in figure 9.2, the root cause being the same, namely, that the error estimates performed by the curve-fitting routine appear to be too optimistic.

There was a considerable scatter in the final results for the coefficient γ_i, the variation being between 0 and about 2%. Although a precise value could not be determined, the upper limit of this range is consistent with values tabulated in table 2.3.

9.2. Time-dependent measurements.

As described in section 3.2, the same Molnar technique (Molnar 1951b) that was used in the previous section to remove the metastable contribution to the total steady-state discharge current can also be used to measure effective values of the diffusion and quenching coefficients D_m and G_m of the metastable atoms – indeed, this was the original use to which Molnar put the technique. The values of D_m and G_m must be considered 'effective' values because the technique does not distinguish between different metastable particles, which may have differing values of these quantities. As is well known, in argon there are two metastable states ($1s_3$ and $1s_5$ in Paschen notation). However, there is much evidence to support the belief that the $1s_5$ state is present under most discharge regimes of present interest at a concentration some ten times larger than the $1s_3$ state (Ellis and Twiddy 1969, Tachibana 1986). The values of D_m and G_m returned by an analysis of the decay of the discharge current may therefore be usefully compared with values obtained for the $1s_5$ state by other means.

It was therefore decided to follow in Molnar's footsteps and attempt measurements of these quantities. It was originally intended to extend these measurements over a greater range of pressures than was addressed by Molnar, partly to investigate whether the two- and three-body quenching processes measured by Ellis and Twiddy (1969) and subsequent authors were evident in the high pressure limit, but also to attempt a measurement of the boundary parameter β described in section 3.1.1. In the event, great difficulties were encountered in performing the measurements. Some of these were of an experimental nature, such as the problem with outgassing of impurities described in section 7.1, but others were problems of a more fundamental nature concerning the Molnar analysis (Molnar 1951a) and its application to plane-parallel electrodes of finite radius. An alternative, separation-of-variables (SOV) approach to the theory of the decay of slow current (described in section 3.2.2) showed that the Molnar analysis was incomplete as described in Molnar's original paper, and that the methods developed by this author for obtaining the free-decay rates from measurements of the slow-current-decay rates produce, in many cases, grossly incorrect results. Some data on the values of the effective

diffusion and quenching coefficients were, however, eventually obtained, the results being broadly consistent with previous measurements.

9.2.1. Difficulties with the measurements.

Because of the concerns with the Molnar theory that arose during the course of the experiments, attention was directed first at the prediction that complex-valued decay rates occur in the decay of slow current under certain discharge conditions, and the effect such terms might have on the analysis of the Molnar experiment. It was decided to investigate this as follows. Recordings were taken of the decay of slow current, using a constant electrode spacing and pressure, but varying the potential difference across the electrodes (and hence the reduced electric field *E/N*). The fundamental rate of decay of the slow current is expected to increase as the field is increased, because the greater field induces a correspondingly larger amount of feedback from secondary electrons ejected from the cathode by metastable atoms. These fundamental decay rates were measured and compared with the approximate predictions of the standard Molnar theory and also with the exact (in principle) predictions of the SOV theory. Two approximations to the Molnar theory were used, one corresponding to equation (3.70) (equation 23 in Molnar 1951a), the other to equation (3.71), which is equaivalent to Molnar's equation 23 in the approximation $i_{s2} \rightarrow 0$. Two sets of data were taken, one at a separation of 1.016 cm, the other at 2.540 cm.

The more crude Molnar approximation is straightforward to apply, since the results depend only on the value of the breakdown parameter $\chi = I_{slow}/I_{total}$. However, in order to perform the calculations required by the other two models, some additional quantities have to be determined. Firstly, the SOV model requires the value of α_i to be known. This coefficient had therefore to be determined at a number of values of *E/N* within the range over which measurements were taken. Several steps were used to calculate these values of α_i. Firstly, the value of *E/N* at which each data value was recorded was plotted against the observed value of χ for that point. These plots are shown in figures 9.8 and 9.9. A line of best fit was drawn through these points. For a number of closely spaced points within the interval of χ in which the data were taken, the appropriate value of *E/N* was interpolated from this graph; the value of α_i at this value of reduced field was then estimated by cubic spline interpolation of the data of Kruithof (1940).

Secondly, the 2-term Molnar approximation requires a knowledge of the amplitude of the second decay term. This is difficult to measure in practice, so values of this

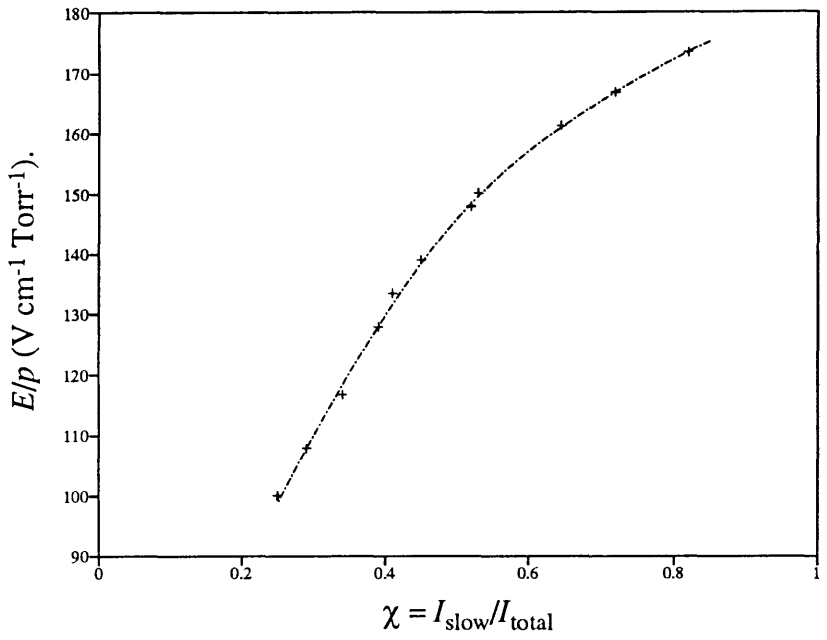

Figure 9.8. The relationship between the reduced electric field *E/p* (normalised to 0 °C) and the breakdown parameter χ. Data were taken at an electrode separation of 0.4 in (1.016 cm) and a pressure of 0.96 Torr. The chained line was fitted to the data points, which are marked by crosses.

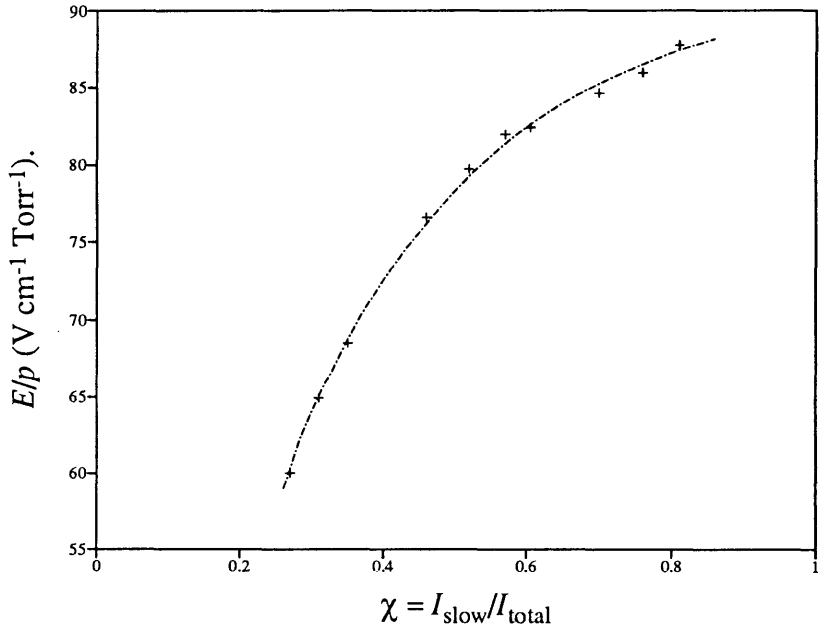

Figure 9.9. This plot is similar to figure 9.8, except that the data displayed here were taken at an electrode separation of 1 inch (2.54 cm) and a pressure of 0.95 Torr.

amplitude at the required values of χ were estimated using the SOV theory. Finally, both the 2-term Molnar approximation and the SOV theory require knowledge of the values of the diffusion and quenching coefficients. For the sake of the exercise, values determined *a posteori* from plots of free-decay rate against π^2/d^2 were used (see section 9.2.2 for a description of these results).

The values of the first, second and third decay time constants predicted by the SOV model at various values of χ, for the smaller value of d, are displayed in figure 9.10.

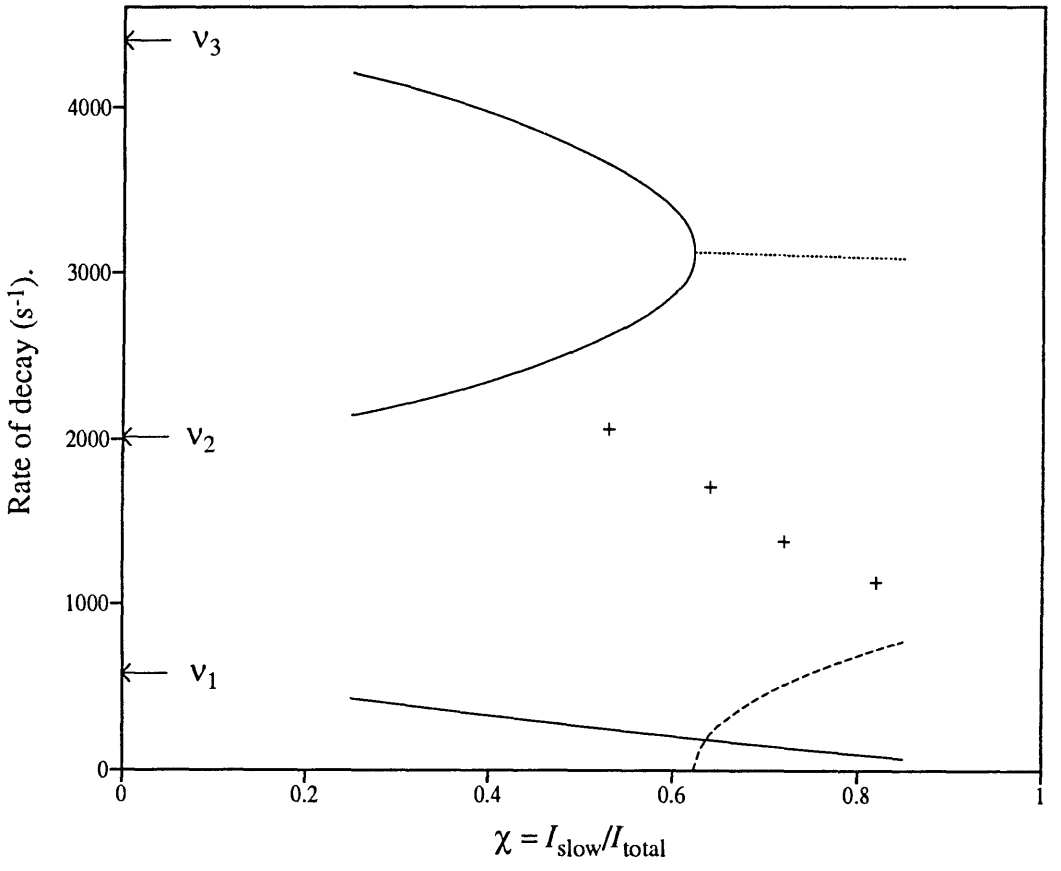

Figure 9.10. The first, second and third decay rates (solid lines) of the slow current decay plotted as a function of the breakdown parameter χ. The electrode separation was 0.4 in (1.016 cm) and the pressure was 0.96 Torr. The values of α_i which were necessary for the calculation of these decay rates were interpolated from the data of Kruithof (1940). In the limit $\chi \rightarrow 0$, the decay rates approach the free-decay rates which are indicated on the left-hand axis of the graph. The 2nd and 3rd decay constants become complex-valued at about $\chi = 0.6$. The dotted and dashed lines represent, respectively, the real and imaginary parts of the 2nd/3rd decay rates at greater values of χ. Four experimental measurements of a higher-order decay rate are also shown (crosses).

It can be seen that the 2nd and 3rd decay rates become complex-valued at about $\chi = 0.6$. However, all three rates trend towards the corresponding free-decay rates in the small-signal limit; also, the fundamental rate decreases toward zero, as expected, in the approach to breakdown. This can be seen more clearly in figure 9.11, in which the theoretical predictions of the fundamental decay rate are compared with the experimental values.

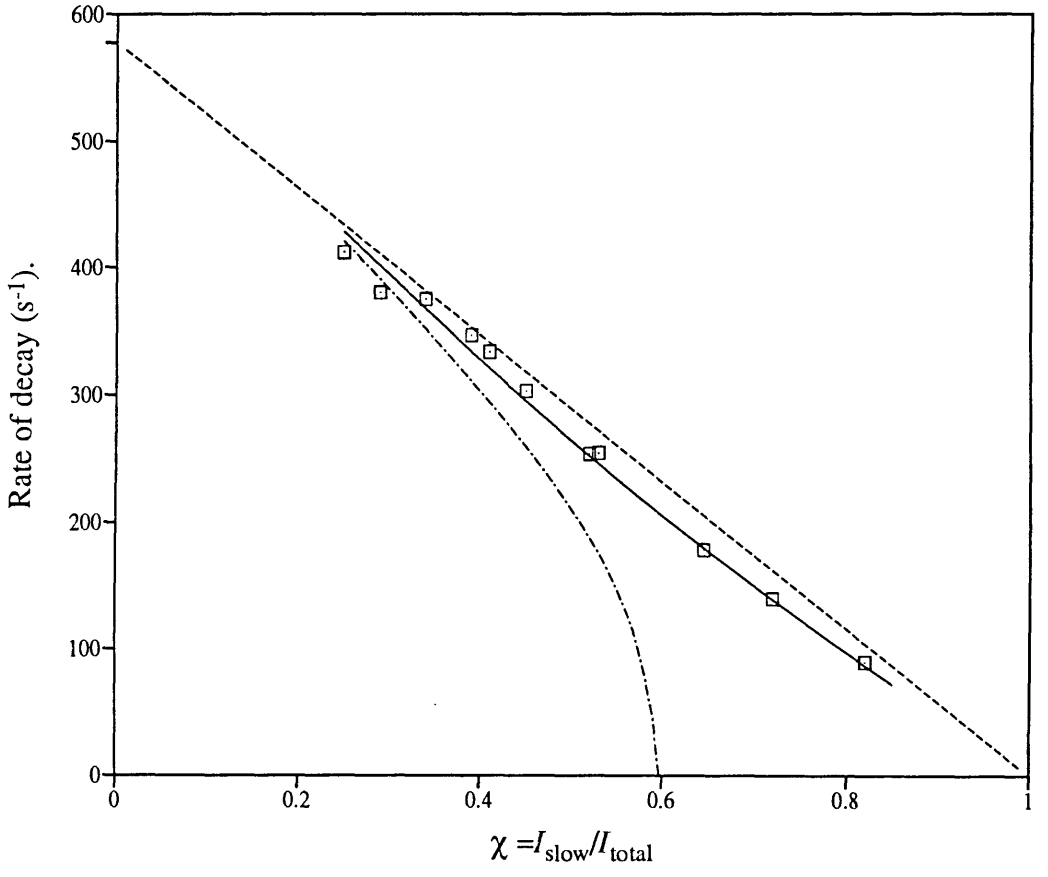

Figure 9.11. This shows measured values of the first decay constant over a range of values of the breakdown parameter χ (small squares). The measurements are the same ones depicted in figure 9.8. Three theoretical curves are also shown. The solid line was calculated by using the analysis of chapter 3, section 3.2.2, and represents an exact value for the simplified form which has been assumed for the generating function $w\alpha_m(\mathbf{r})n_e(\mathbf{r})$ in equation (2.15). The chained curve represents the values obtained by using equation (3.70) (equation 23 in Molnar 1951a), whereas the dashed line is the solution found by using equation (3.71) (that is, Molnar's equation 23 in the limit that $i_{s2} \rightarrow 0$). The value of $\rho = \nu_2/\nu_1$ ('β' in Molnar's notation) was obtained by using the values of D_m and G_m obtained *a posteori* from later experimental measurements.

The SOV line is seen to be not too far from the 1st-order Molnar approximation, although the data points clearly favour the SOV curve. The 2-term Molnar approximation is fair for small χ but fails completely at χ greater than about 0.5. The fundamental reason for this is the unbounded increase in the amplitude of the second and third decay terms as their respective time constants approach the point of degeneracy between the real-valued and complex-valued states (see section 3.2.2.4).

Similar results are observed at the large electrode spacing (figure 9.12). If anything, the failure of the 2-term Molnar approximation is even more severe.

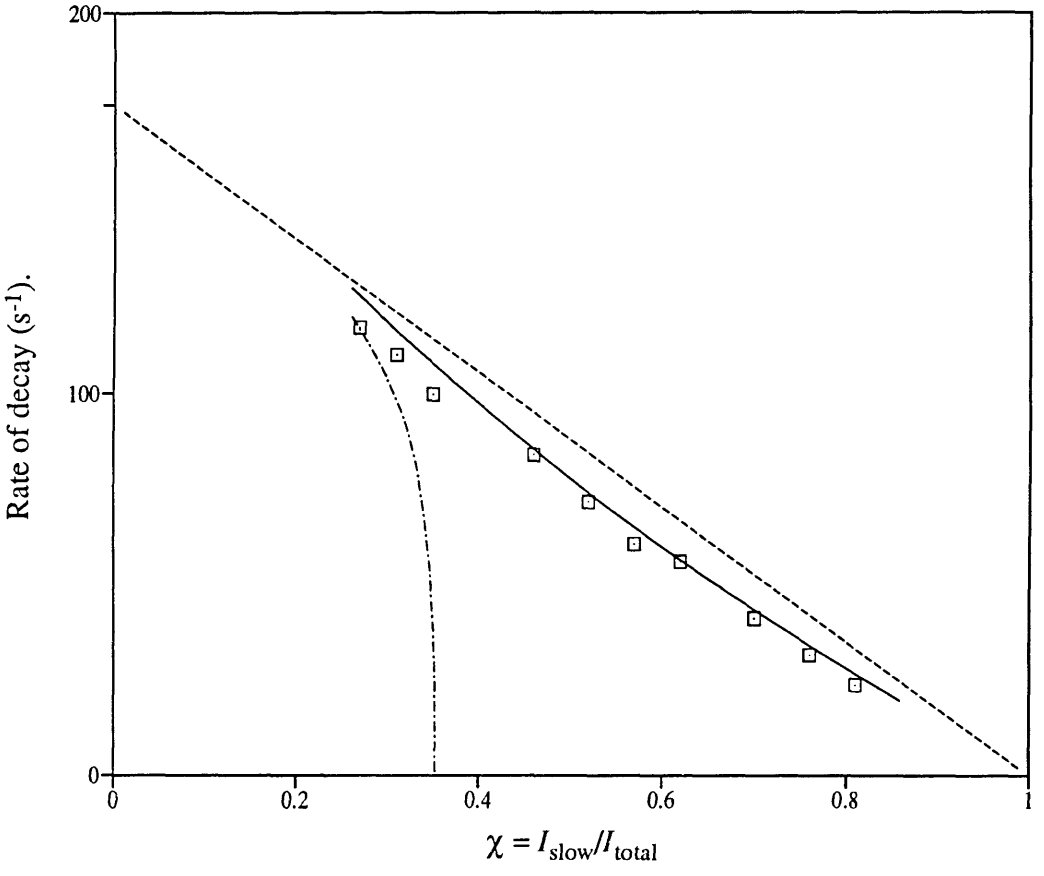

Figure 9.12. This plot is similar to figure 9.11, except that the data displayed here were taken at an electrode separation of 1 inch (2.54 cm) and a pressure of 0.95 Torr. Under these conditions, the second and third decay rates become complex-valued at about $\chi = 0.35$.

An attempt was then made to search for experimental evidence of an oscillatory component in the decay of slow current at large values of χ. However, unequivocal

evidence could not be found. Many curves appeared to the eye to contain a sinusoidal component at the base of the 'pedestal', but quantitative agreement with the predictions of the SOV theory is lacking. An example of such a signal is shown in figure 9.13. (Note that it is shown in section 3.2.2.3 that the oscillatory decay, although technically a 'decaying sinusoid', is likely to be heavily damped. Obvious oscillations in the detected signals are therefore unlikely to be observed.) An attempt to fit an exponential to such signals produced curious results, which are shown on figure 9.10. At the lowest value of χ at which such a fit could be performed, the time constant was not too far from that predicted by the SOV theory for the second decay term, which at that point is expected still to be real-valued. However, at larger values of χ, the measured time constants decreased smoothly, contrary to expectations, and bear no obvious relationship with the predicted values. Figure 9.13 provides visual confirmation that these too-slow decays are real, and

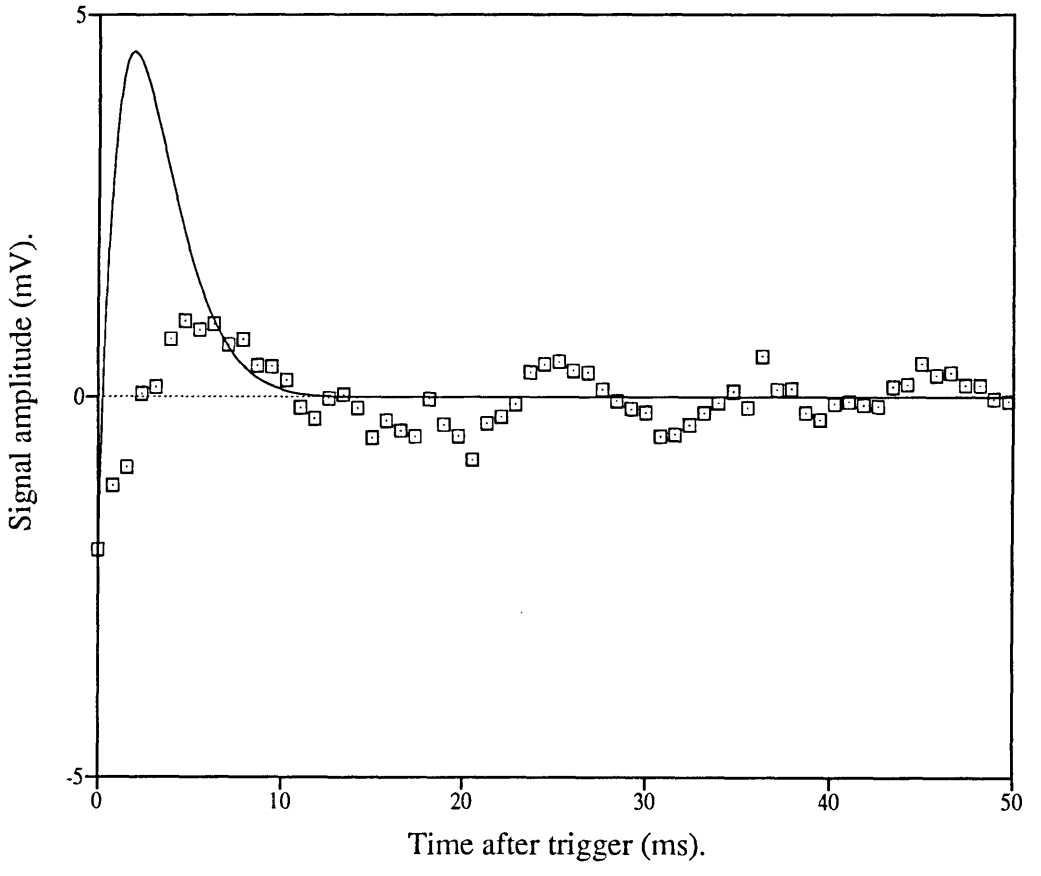

Figure 9.13. Higher decay terms of the slow current at d = 2.54 cm and p = 0.954 Torr. The solid line represents the predicted form of the complex second and third decay terms; the boxes represent binned averages, each of 20 samples, of the slow current signal after subtraction of the fundamental decay.

not just an artifact of the fitting procedure: the rate of decay of the negative-amplitude term in the data points is seen in this diagram to be several times slower than that of the theoretical curve.

Bearing in mind the fact that only four data points were taken, that the amplitudes of these components were very small and hence that the measurements were difficult to make, and that the fitting of multi-exponential data is a dubious undertaking at the best of times, the role of chance in the apparent trend of these points should perhaps not be underestimated.

Two other curious effects were noted. Both occurred at small values of the electrode separation *d*. The first of these anomalies is the presence of a decay component with a time constant (of about 5 msec) which was found to be only weakly dependent on *d*. This component makes an appearance at an electrode separation of about 0.4 inches, and quickly comes to dominate the decay of the slow current at smaller separations. Its presence limits the accuracy with which D_m may be determined and makes it impossible to perform the small-*d*, high *E/N* measurements that are necessary to determine the value of the boundary parameter β. No definite explanation is known, but one possible cause is an enhanced production of metastable particles at the edges of the electrodes. At the high values of *E/N* that are necessary to achieve a significant amount of slow current at these small separations, the discharge regime is firmly to the left of the Paschen minimum (see figure 9.17). Because the production of metastables may be assumed to be most efficient at this minimum, 'long-path' effects may produce a significant concentration of metastables at the edges of the electrodes. Although a calculation of the diffusion dynamics of particles about the rounded edges of the electrodes is bound to be a complicated undertaking, one may estimate that the value of the diffusion length Λ might be somewhere near to the radius of the electrode bevel (~ 1 cm in the present case), and furthermore, that it is likely to remain approximately constant over a range of electrode separations Δd such that $\Delta d < \Lambda$. In other words, if the diffusion length at the electrode edges was 1 cm when the electrodes were in contact, it would have increased by only 20% at $d = 0.2$ cm.

The final anomalous effect was also observed during attempts to measure the boundary parameter β and is so far without a satisfactory explanation. It is the occasional presence, at electrode separations smaller than about 1 mm, of strongly oscillatory signals after the cessation of the primary current. An example is shown in figure 9.14, with the remaining slow decay subtracted to show the oscillations more clearly. Several features of

these signals were observed. Firstly, the period of the oscillations remains approximately constant, regardless of the value of d, and is suspiciously close to 10 ms (ie, to half the period of the mains power supply). The amplitude was observed to increase as d was decreased, which is consistent with the capacitive coupling of a noise signal across the electrodes. However, the period does not seem to be exactly equal to 10 ms, as it would have to be if the phenomenon was simply due to noise from the mains voltage. Also, the noise hypothesis does not explain the decay of the oscillation envelope. Alternatively, the signal could be due to inductive ringing in the external circuit. However, if this is the case, it is strange that the capacitance of the electrodes, which is approximately equal to $1.8/d$ pF (for d in cm), appears to have no effect on the period of the oscillations.

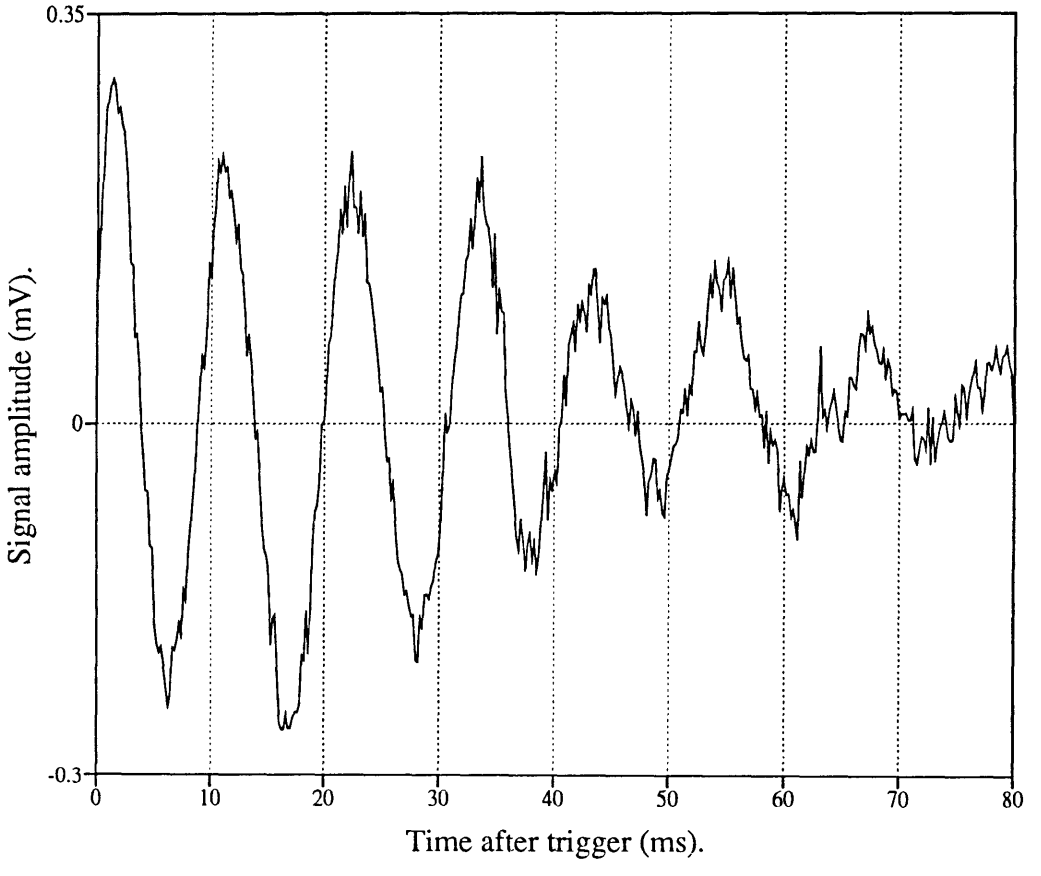

Figure 9.14. A typical oscillation seen on traces taken at electrode separations of less than 1mm. A double exponential term $V(t)$ given by

$$V(t) = -17.72 + 0.7\exp(-t/18.755) + 6.3\exp(-t/2.337)\ \text{mV}$$

has been subtracted from the raw data. (Times are in msec.)

9.2.2. The diffusion and quenching coefficients.

These were evaluated at a single value of the gas concentration N by use of the method described in Molnar (1951b). At each value of the electrode separation d, the potential difference was adjusted so as to produce a significant amplitude of 'slow' current. The signal passed by the discharge as the source of primary current was switched on and off was amplified and then recorded on a digital storage oscilloscope, as described in section 7.2.1. A function consisting of either one or a sum of two exponentials was fitted to the data by the procedure described in section 8.3, in order to determine T_1, the fundamental time constant of the decay of slow current. The first-order approximation to Molnar's theory (ie, equation 3.71) was then used to retrieve the fundamental 'free-decay' time constant τ_1 from the measured values of T_1 and the breakdown parameter χ.

It was necessary to correct the values of τ_1 for the variation with time of the quenching rate G_m, which occurred as a result of the constant outgassing of impurities from the chamber walls (see section 7.1). This was done as follows. At the commencement of a set of measurements, as soon as possible after the chamber was isolated from the vacuum pump and gas admitted, the electrodes were opened to their widest spacing (1 inch = 2.54 cm). The potential difference was adjusted so as to bring the value of the breakdown parameter $\chi = I_{slow}/I_{total}$ to about 0.5. This ensured that the total current was large, and therefore that the signal-to-noise ratio was comfortably high. The time constant τ_1 of the free decay at this separation was then determined by the method described above. At intervals during the measurements, the electrode spacing and potential difference were returned to these initial values, and the measurement was repeated. A graph of the increase in the time constant at this reference separation allowed the increase in G_m with time to be determined. An example of such a plot is shown in figure 9.15.

After correction for outgassing, the decay rates $\nu_1 = 1/\tau_1$ were plotted as a function of $(\pi/d)^2$. As described in Molnar (1951b) and also section 3.1.2, this should yield a linear plot with a slope equal to D_m and a y-intercept of G_m. The plot is shown in figure 9.16. (Note that the scatter in the data values is, as was the case in figures 9.2 and 9.7, much larger than the uncertainties returned by the fitting procedure.) The two coefficients were obtained by an ordinary least-squares fit to the data points. The diffusion coefficient is compared with published values in table 9.1. Very good agreement is obtained with all previous results within the quoted uncertainties.

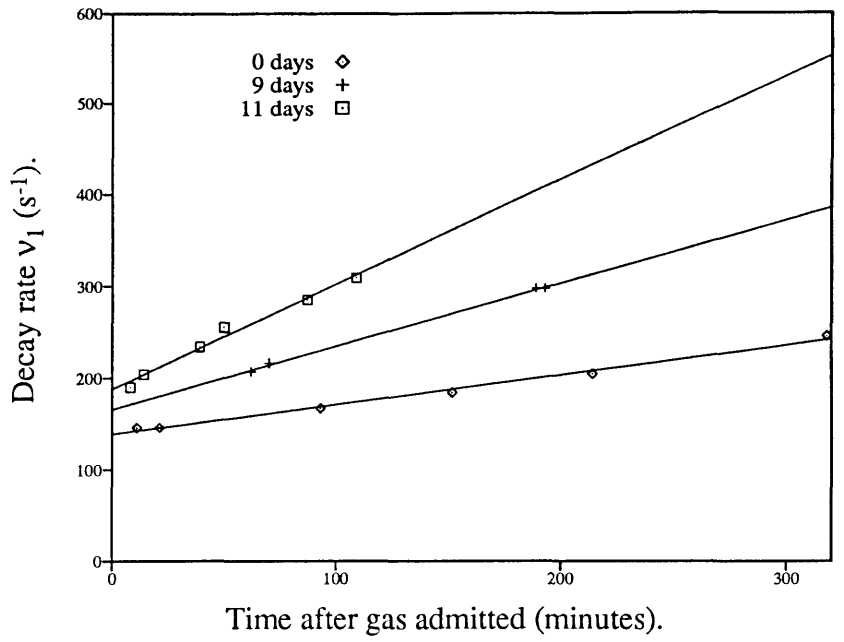

Figure 9.15. The increase in the rate of quenching of metastable atoms due to outgassing. The legend gives the time in days after the titanium getter was applied.

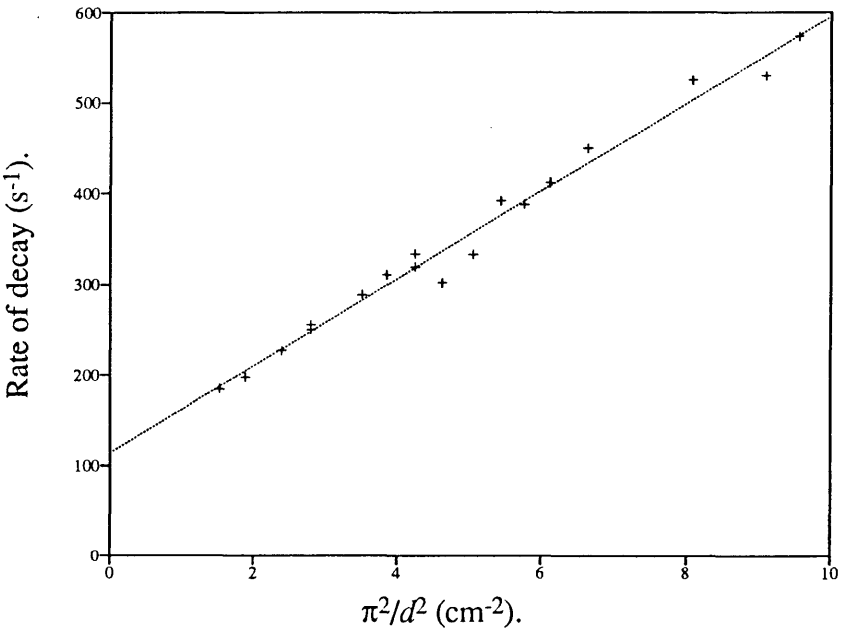

Figure 9.16. A plot of the fundamental free-decay rate ν_1 against the square of π/d (crosses), d being the electrode separation at which the reading was taken. The dotted line was fitted to the points by a standard linear regression. The y-intercept of this line gives the value of the volume quenching coefficient G_m, whereas the slope is equal to the diffusion coefficient D_m. The values of ν_1 were calculated from measurements of the first time constant of the decay of slow current, after these were corrected for drift in G_m due to outgassing. Equation 3.71 was used for the conversion from slow current rate to free-decay rate.

Table 9.1. Values of the diffusion coefficient of argon $1s_5$ metastables at 300 K.

Reference	$D_m N$ (10^{18} cm^{-1} s^{-1})
Molnar[a] (1951b)	1.45 ± 0.13
Phelps & Molnar (1953)	1.74
Futch & Grant (1956)	1.64 ± 0.14
Ellis & Twiddy (1969)	1.66 ± 0.07
Kolts & Setser (1978)	1.8
Wieme & Lenaerts (1980)	1.48 ± 0.12
Present work[a]	1.57 ± 0.05

Notes:

a: The metastable atoms in these cases are presumed to be mostly in the $1s_5$ state.

At 1 Torr and 296 K, Ellis and Twiddy determined the rate of self-quenching to be 51 s^{-1} in pure argon. This is about 60 s^{-1} below the present value of 114 ± 8 s^{-1}. The difference is consistent with about 130 ppm CO, 50 ppm N_2, 9 ppm O_2 or 4 ppm H_2O (Kolts and Setser 1978). These figures are mostly higher than the value of 5 ppm quoted for the argon used in the present experiment (Matheson research grade). Note, however, that all three lines in figure 9.15 converge to a point about 1 hour before the admission of gas to the chamber. The meaning of this is not known. If this point of convergence is taken as representing the true quenching rate in the unmodified gas, the difference between the present value for G_m and that of Ellis and Twiddy falls to about 20 s^{-1}. The concentrations of common impurities that are necessary to produce this amount of quenching are much closer to 5 ppm.

9.3. Electrical breakdown in argon.

The absorption measurements described in the next chapter are difficult to make because the concentration of metastable excited states in the pre-breakdown regime is very small. Because secondary electrons ejected from the cathode by metastable impact play such a large role in the occurrence of breakdown in argon, the concentration of these

states is likely to be at an optimum level when the breakdown voltage is minimized. This can be shown in a more quantitative fashion as follows. Taking equation (2.10) as a starting point, the following equation was derived in section 3.2.2.5:

$$\alpha_i d_{bd} \sim \alpha_i d_0 + \ln[1+1/\gamma], \tag{9.1}$$

where α_i is Townsend's first ionisation coefficient, d_{bd} is the separation of the electrodes at breakdown, d_0 is the 'non-equilibrium distance' defined in section 2.1 and γ is the generalised secondary coefficient. The coefficient γ contains a constant part representing the contribution of ions and a d-dependent part representing the contribution made by metastable particles. Equation (9.1) can be written as

$$V_{bd} \sim V_0 + \frac{E/N}{\alpha_i/N} \ln[1+1/\gamma], \tag{9.2}$$

where V_{bd} is the breakdown voltage, E the electric field and N the gas number density. The voltage V_0 is related to d_0 by $V_0 = Ed_0$. Both α_i/E and V_0 are slowly varying functions of E/N (Kruithof 1940), in other words, of V_{bd}/Nd_{bd}; clearly, then, if γ were constant, V_{bd} would be a function of d_{bd} only. This is called 'Paschen's law' or 'the Principle of Similarity' (eg Meek and Craggs 1953). However, in cases where part of the secondary ionisation is due to metastable particles, γ varies with both N and d, and Paschen's law is therefore only approximately followed.

In order to identify the conditions at which the minimum in V_{bd} occurs, this voltage was measured for a variety of values of the electrode spacing and gas pressure. The results are shown in figure 9.17. It can be seen that, as predicted above, Paschen's law is only approximate in the case of argon.

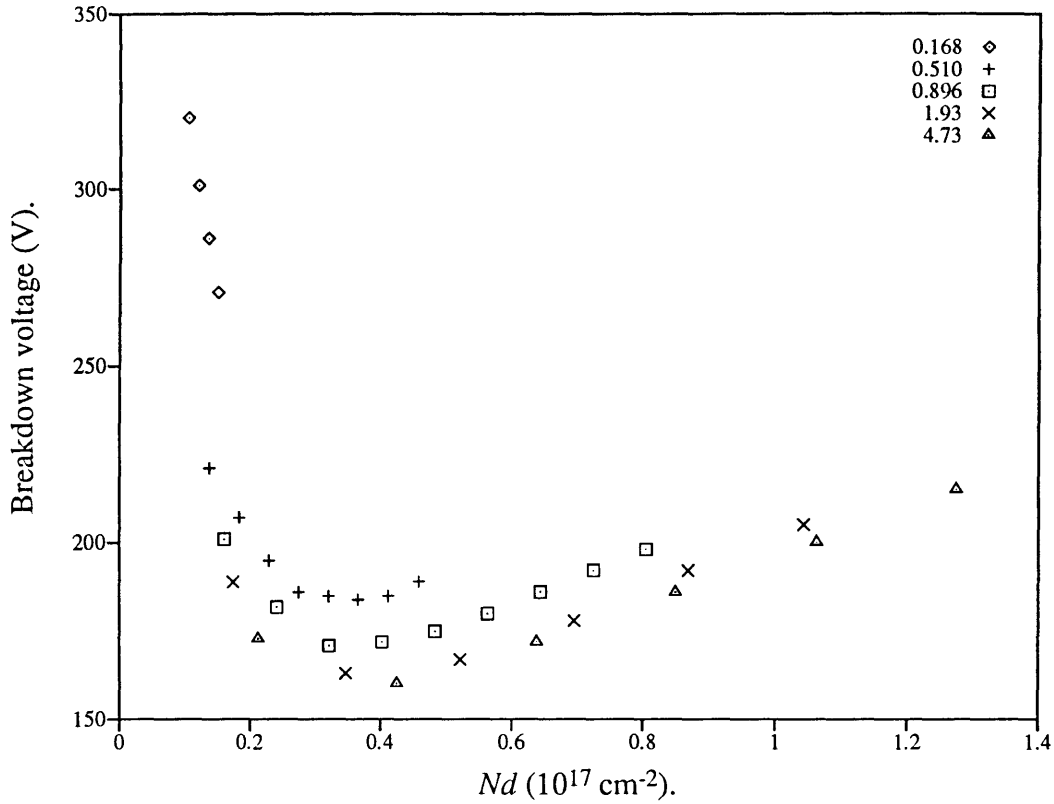

Figure 9.17. The variation in breakdown voltage with the product Nd in argon (N being the gas number density and d the electrode separation). The numbers in the legend are pressures in Torr, normalised to 0 °C.

10. Optical absorption measurements.

As described in the introductory chapter, optical absorption measurements have the potential to return information about a number of aspects of the pre-breakdown discharge in argon. Some of these possibilities are discussed in greater depth in chapters 3 to 6. Broadly speaking, these avenues of investigation fall under five heads: (i) examination of the saturation behaviour of the absorption coefficient at high light intensity; (ii) measurement of the diffusion and volume quenching parameters without the complications inherent in a Molnar-style experiment; (iii) obtaining information about the rates of production and surface quenching of metastable atoms from their steady-state concentration profiles; (iv) measurement of some of the electron transport parameters, and (v) the determination of the primary ionisation coefficient without needing to consider the contribution from other sources of ionisation.

A number of measurements of the light absorbed by $1s_5$ metastable atoms were performed towards the end of the study period. The intention behind these was to demonstrate these experimental and analytical techniques, and to compare experimental distributions with the models developed in chapters 5 and 6, rather than to embark on a comprehensive program of measurements of the discharge parameters. The results of most of the experiments are in qualitative agreement with the predictions of theory; the degree of numerical agreement is discussed below.

As described in chapter 7, the measurements were performed by directing a thin beam of radiation from a semiconductor laser through the discharge volume in a direction parallel to the electrode planes. The position of the beam can be varied by moving the entire laser carriage. The transmitted light is detected by a photodetector on the other side of the discharge chamber, which is moved in concert with the laser. The amplified photovoltage is recorded on a digital storage oscilloscope; this allows many traces to be averaged, for the purpose of increasing the signal to-noise ratio. The result can be transferred to a computer for further digital processing. The absorption signal is generated by pulsing either the potential difference across the electrodes, the ultraviolet light (the source of the primary current), or both. Pulsing or chopping the potential difference is the preferred technique for all of the areas of investigation listed above. In the case that the diffusion and volume quenching of the metastable atoms are being examined, chopping the voltage permits the relevant parameters to be measured during 'free decay'. In the case of the other types of measurement, voltage chopping permits a greater number of cycles to

be performed in a set time, because the metastable atoms are cleared from the discharge much more rapidly than they would be if the voltage was maintained after switching the lamp off. This is because the potential difference causes some regeneration of the metastables through the continued drift of secondary electrons. Voltage chopping also permits an over-voltage to be applied during the 'on' part of the cycle, which allows the exploration of discharge regimes that would otherwise be inaccessible.

An example of a 'raw' signal is shown in figure 10.1. The following figure shows the same signal after averaging many samples. The signal to noise ratio has increased by about a factor of 40. As described in section 7.2.2.2, it is necessary to interpose a high-pass filter between the photodetectors and the differential amplifier. This has the effect of imposing a noticeable 'droop' on signals recorded at timebases of greater than a few milliseconds. A digital technique is described in section 8.1 for removing this distortion. This technique has been applied to the data in figure 10.2.

10.1. Saturation of the absorption coefficient.

The desire to obtain spatially resolved information about the concentrations of excited states, together with the necessity of maintaining a reasonable signal-to-noise ratio,* require that the intensity of the laser radiation be relatively large. In this case, it may not be possible to ignore saturation effects when calculating the absorption coefficient. The saturation dynamics of a thin beam are discussed in section 4.2.2, in which it is shown that the absorption coefficient k is a function of laser power P of the form

$$k = \frac{k_0}{\sqrt{1+P/P_{sat}}}, \tag{10.1}$$

where k_0 is the small-signal absorption coefficient given by equation (4.19) and P_{sat} is the saturation power. Provided that the absorber is optically thin, a similar expression holds for the integrated absorption κ which is defined, for a beam propagating in the y direction, by

$$\kappa = \int dx\, k(x). \tag{10.2}$$

* If this is to be achieved, the laser power must be maintained at a reasonable level, because the fractional amplitude of the electrical shot noise from the photodetectors is inversely proportional to the square root of their DC output.

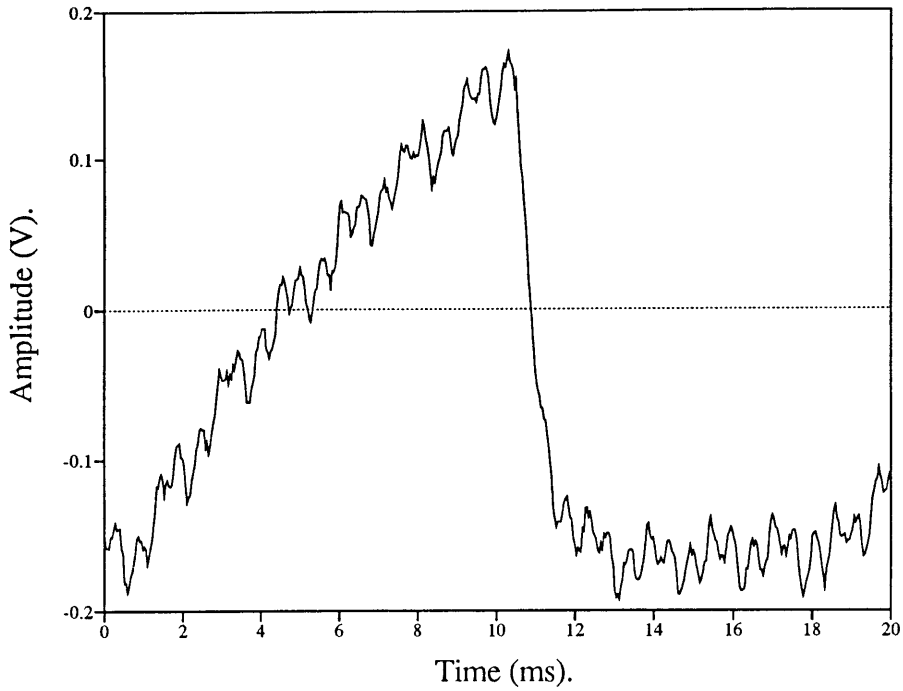

Figure 10.1. A typical absorption signal. The discharge commences at about 1 ms (and again at 19) and ends at about 10.5 ms.

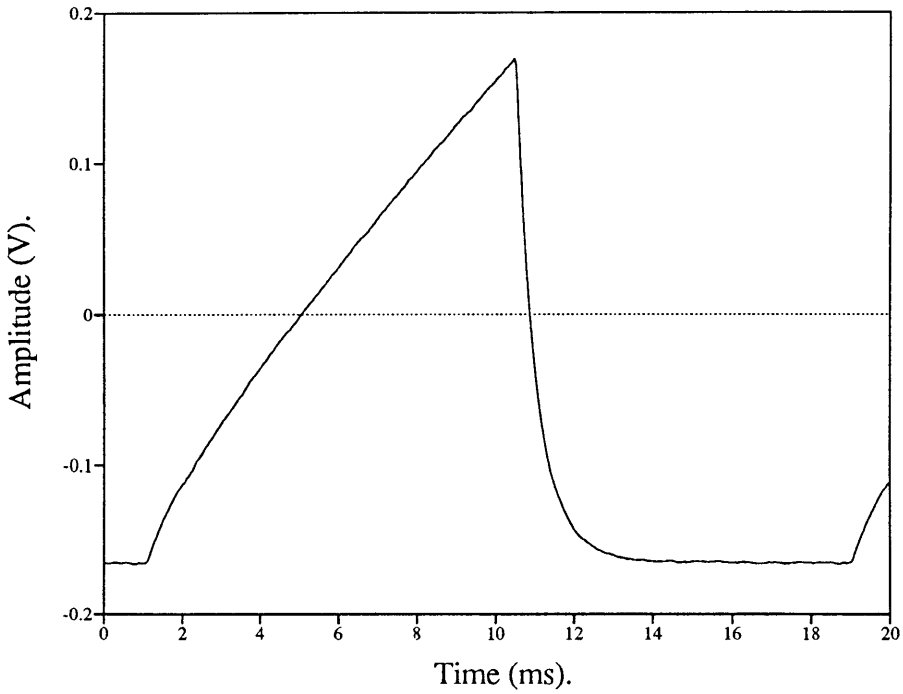

Figure 10.2. An average of 2000 such signals, which has, in addition, been 'undrooped' by the method described in section 8.1. The nature of the rise in the concentration of metastable atoms can be clearly seen, as well as the exponential shape of the decay.

The change in the integrated absorption as the laser power was varied was investigated. The results are shown in figures 10.3 and 10.4.

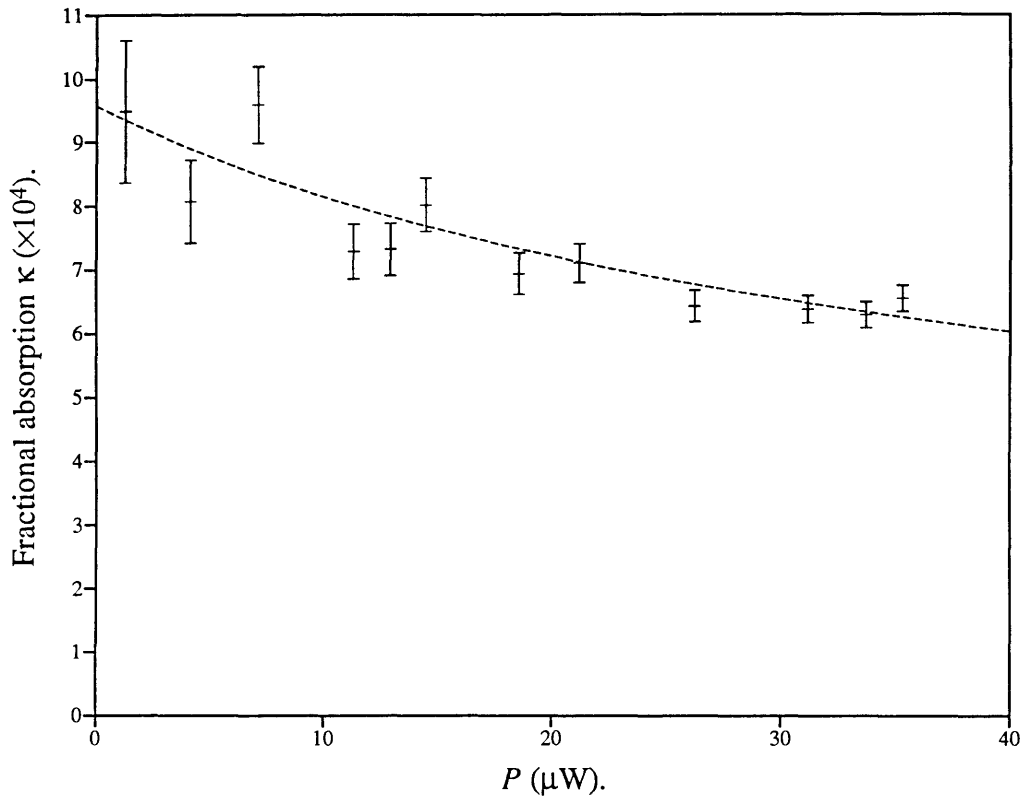

Figure 10.3. Saturation of the $1s_5$ - $2p_9$ transition as P, the power in the main laser mode, is increased. The beam radius was 0.8 mm. The dashed curve is the function

$$\kappa = \frac{\kappa_0}{\sqrt{1+P/P_{sat}}},$$

with $\kappa_0 = 9.57\times10^{-4}$ and $P_{sat} = 26.2\mu W$. These parameters were calculated by fitting a line to the data of figure 10.4.

Figure 10.3 shows the raw absorption values. Some downward trend is evident, following the general shape predicted by equation (10.1). However, a better way to measure the two free parameters is to manipulate the data so that a linear plot can be performed. This has been done in figure 10.4.

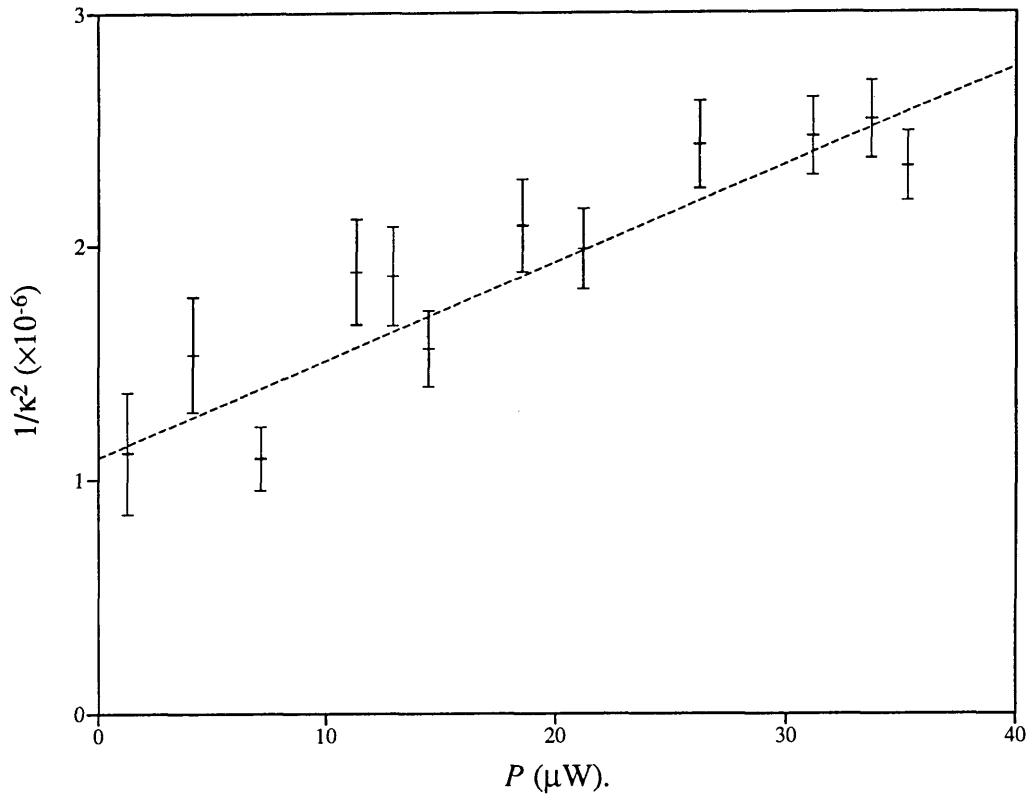

Figure 10.4. A plot of $1/\kappa^2$ against P for the $1s_5$ - $2p_9$ transition. The theory of chapter 4 can be used to show that such a plot should yield a straight line with an intercept equal to $1/\kappa_0^2$ and a slope equal to $1/\kappa_0^2 P_{sat}$. The dashed line was fitted to the data by a weighted least squares procedure (Weisberg 1980).

The data points in this figure are consistent with the linear theoretical prediction. The value of 26.2 μW measured for the saturation power is not in agreement with the value predicted by equations (4.28) and (4.81), which is only 0.2 μW for a beam of radius 0.8 mm. However, this analysis did not include effects due to cross-relaxation of atoms between velocity classes. As is mentioned in section 4.2.1.2, this may increase the saturation intensity or power by a significant amount.

In section 4.3, it is pointed out that an intense beam may also perturb the rate of decay of metastable particles. An attempt was made to measure such a perturbation, the results of which appear in figure 10.5. No systematic trend can be seen; nor is such an effect apparent in the data of the next section. However, the process must occur to some degree. Evidence of this was provided by the observation of an optogalvanic effect in the discharge very close to breakdown. As the laser wavelength was tuned through the

transition, the current passed by the discharge under these circumstances typically decreased by about 10 percent. Note that the change in decay rate should not be expected to be of similar size, because the discharge is particularly sensitive to disturbances near to breakdown, and small perturbations may be greatly magnified.

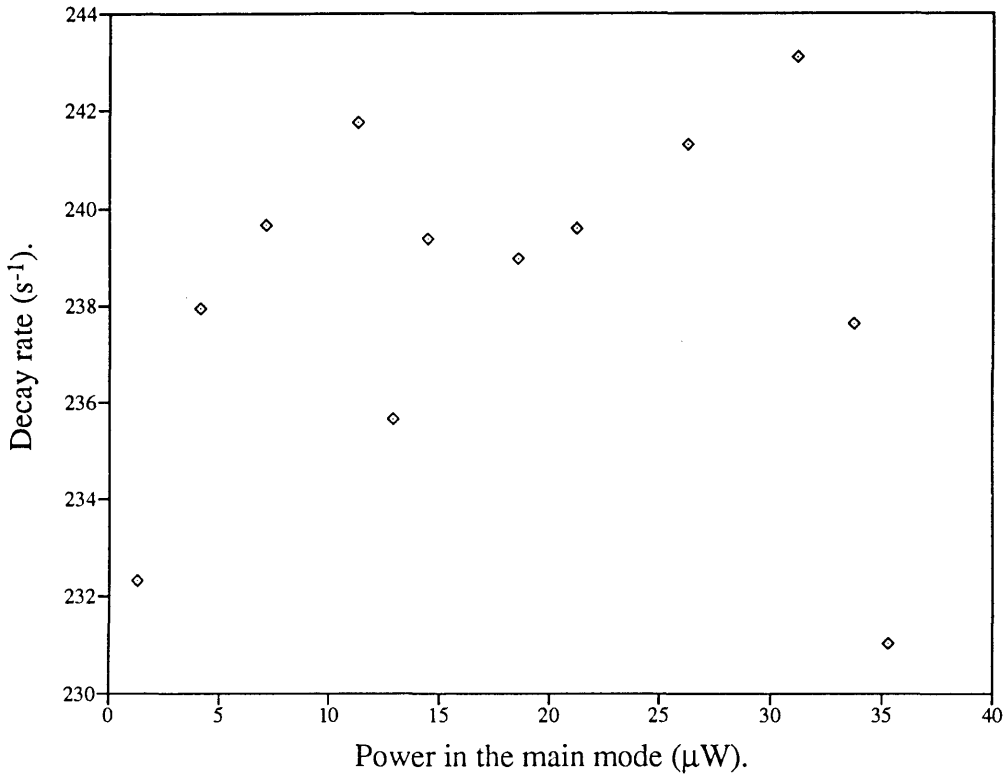

Figure 10.5. The rate of decay of the concentration of $1s_5$ states as a function of laser power. Note the suppressed zero on the ordinate.

10.2. Measurement of the diffusion and quenching coefficients.

A discharge between moveable, plane-parallel electrodes, monitored by optical absorption, ought to provide an excellent opportunity to measure the diffusion, volume quenching and boundary coefficients with high accuracy. However, there was an unexpected problem, the nature of which is well demonstrated by the points on figure 10.6. It can be seen that the slopes of the fundamental decay, although close to the theoretical curve at large electrode separations, diverge smoothly as the separation is

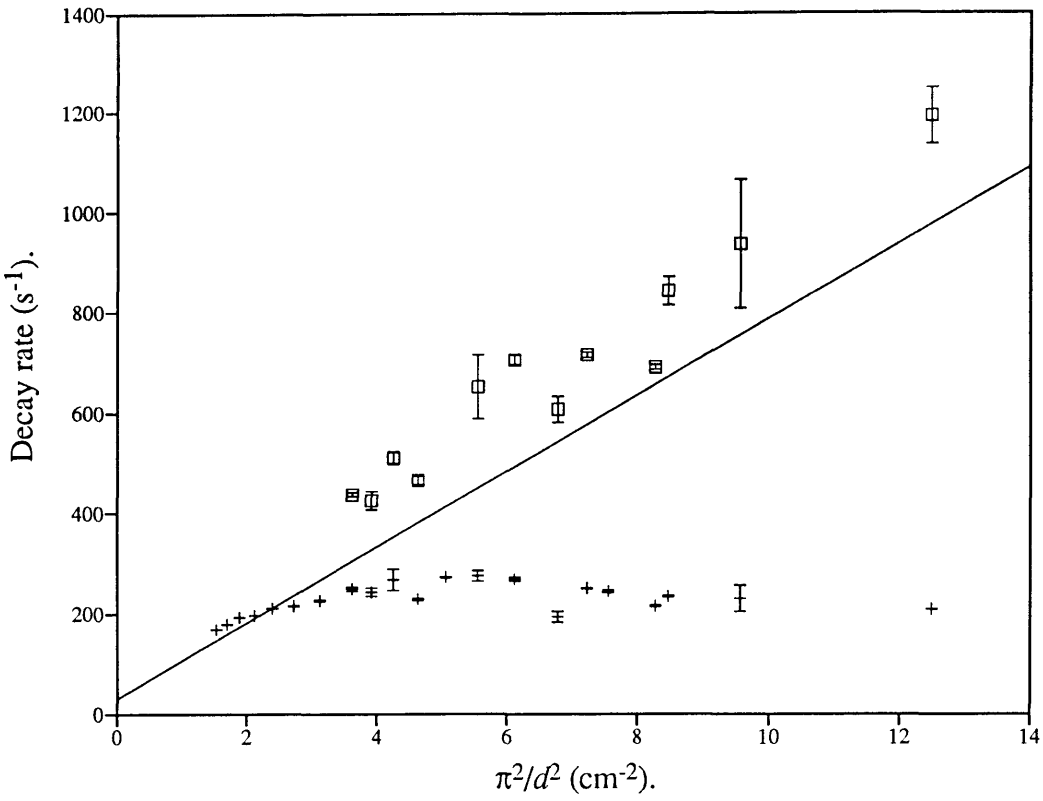

Figure 10.6. The rate of decay in the concentration of argon $1s_5$ state atoms, plotted as a function of π^2/d^2, where d is the electrode separation. According to the theory described in section 3.1.2, the result ought to be a straight line. The crosses represent measurements of the fundamental decay mode, whereas the squares give the decay rates of the next highest mode, where this could be determined. The solid line shows the expected result, using the values of Ellis and Twiddy (1969) for the diffusion and quenching coefficients. The pressure and temperature were 0.7 Torr and 300 K respectively.

reduced. At some point secondary components appear in the decays, which have time constants much closer to the expected values than those of the first components. The explanation for this is as follows. In order to generate a large signal, a considerable overvoltage must be applied during the 'on' time of the discharge. As the electrode separation is decreased, *Nd*, the product of the gas number density times the separation, may move onto the left-hand side of the Paschen curve shown in figure 9.17. In this region, the breakdown voltage is lower between the edges of the electrodes than it is at the centre of the electrodes. It seems likely that, under these conditions, the bulk of the metastable particles will be generated at these edges. When the discharge is terminated, these are free to diffuse radially away from the electrode surfaces, and hence will decay at a lower rate which is only weakly dependent on the electrode separation. The absorption

decay signal will therefore be expected to contain a large component with a time constant which is nearly independent of the separation d, with a small-amplitude component which has the 'correct' decay rate. This is exactly what is observed. A similar phenomenon is discussed in relation to measurements of the decay of the discharge current in section 9.2.1.

The uncertainties in the 'second slopes' are relatively large because of the difficulty in fitting these components. It therefore seems unlikely that the optical absorption technique can be used to obtain accurate measurements of the diffusion and quenching coefficients at low pressures, at least in the present apparatus. Unfortunately, this is exactly the regime in which the diffusion coefficient becomes significant. However, a successful measurement was made at a somewhat larger pressure. This is shown in figure 10.7.

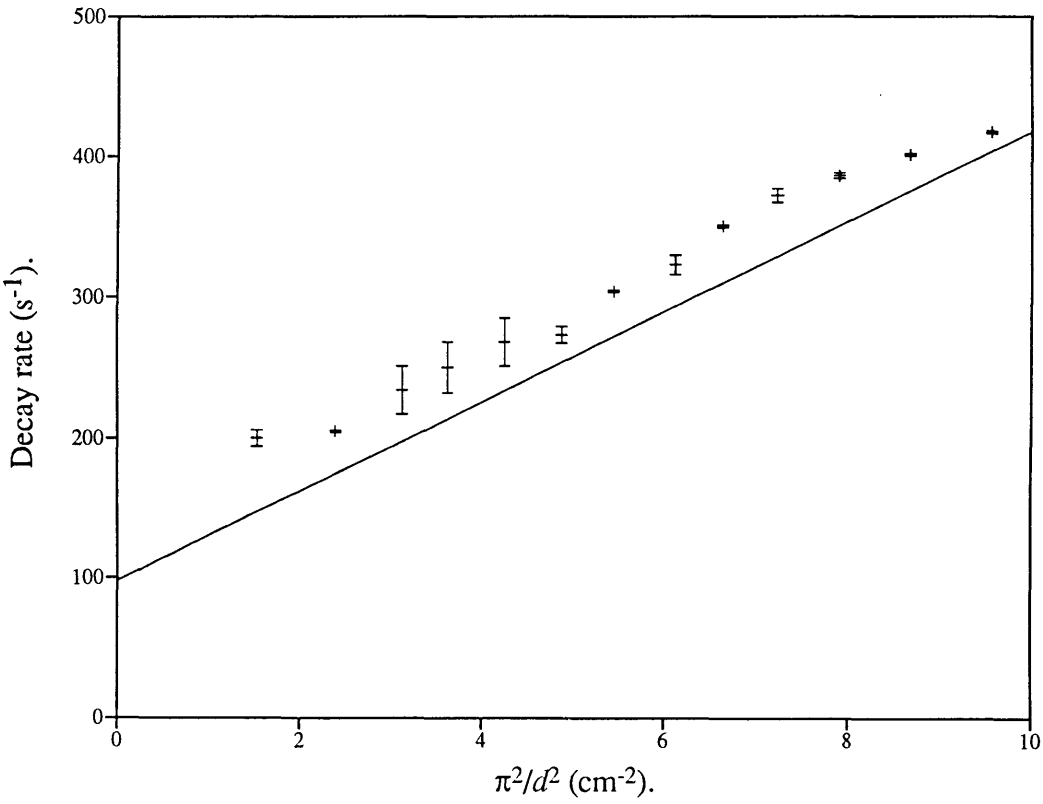

Figure 10.7. A similar plot to that in figure 10.6, except that the pressure here is 1.61 Torr at 300 K. The solid line again represents the prediction of Ellis and Twiddy (1969).

Because of these difficulties at low pressure, no measurements were attempted of the boundary coefficient β described in section 3.1.1.

10.3. Steady-state concentrations of metastable atoms.

As described in chapter 6, it is possible to deduce the value of the secondary ejection efficiency coefficient γ_m from a relatively small number of measurements of the concentration of metastables. In addition, it is possible to calculate the value of α_m as well, since the product $\alpha_m\gamma_m S(d)$ is given by equation (3.91) in terms of the relatively well-known parameters α_i, D_m and G_m. The coefficient $S(d)$, which represents the amplification of the current due to ion-ejected secondary electrons, is equal to the ratio between $I(d)$, the discharge current at separation d, and $I(d_0)$, the current at the effective non-equilibrium separation (provided both measurements are made at the same value of reduced electric field E/N).

Measurements of the concentration of $1s_5$ metastables were performed in a quasi-steady-state regime by allowing the 'slow' part of the discharge current to approach saturation during the 'voltage on' cycle. The $1s_5$ - $2p_9$ transition at 811.5 nm was used. A chain of measurements was made along transects in both axial and radial directions. (An 'axial' transect is defined as a series of measurements at different values of z but $y = 0$; a 'radial' transect is a series performed at several values of y at constant z. The coordinate system is given in figure 3.1, page 23. All measurements were taken with the laser light propagating in the x direction.) These are shown in figures 10.8 and 10.9 on the next page.

The concentration of $1s_5$ atoms along the radial transect could easily be determined by performing an Abel inversion on the data in figure 10.9, but the present author does not consider that this would be particularly informative. An approximate value for the maximum concentration of $1s_5$ state atoms can be obtained from figures 10.8 and 10.9 as follows. The maximum integrated absorption seen in figure 10.8 is about .0015, whereas the half-width of the central 'bulge' in concentration is about 3 cm. Dividing the first figure by the second, and dividing again by the $1s_5$ - $2p_9$ cross-section listed in table 4.4 on page 95, gives an average concentration of about 5×10^7 cm^{-3} (ie, about 1.5 atoms per billion are in the $1s_5$ state).

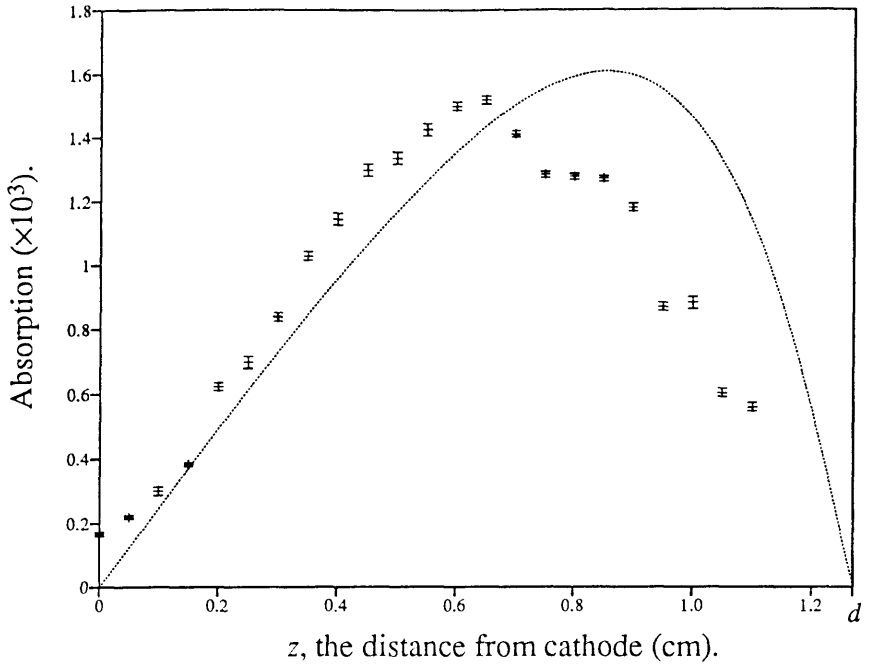

Figure 10.8. The steady-state optical absorption due to argon $1s_5$ atoms, measured along the axis of the discharge. The dotted line represents the values returned by the model of chapter 6. The pressure was 0.97 Torr at 298 kelvin, the discharge current was maintained at 200 nA and the value of the reduced electric field *E/N* was 439 Td.

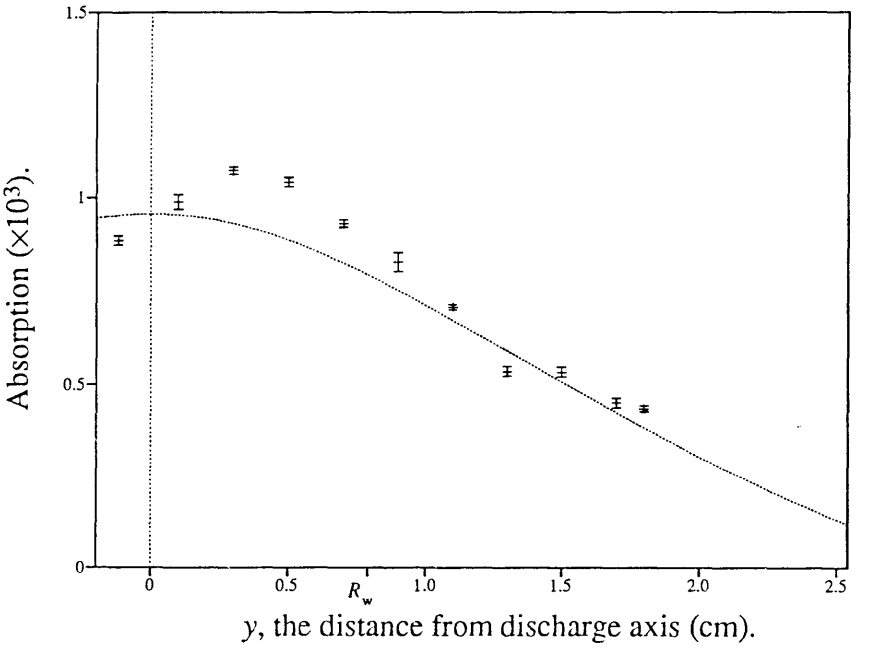

Figure 10.9. Measurements of the $1s_5$ optical absorption across a radial transect at 0.4 cm from the cathode. The electrode spacing and all other conditions were the same as those of the previous figure.

It will be noted that the points in both figures are scattered more widely than the uncertainties in the data would lead one to expect. This is due to difficulties in keeping the laser wavelength centred on the transition of interest, whereas the error bars solely represent uncertainties in fitting curves to the absorption data. The scheme by which the laser is locked to the absorption line is described in section 7.2.2.1. The wavelength is modulated, producing a modulation in the absorption of a reference beam which passes through a wavelength standard and into a monochromator and photomultiplier. The result is detected by a phase-sensitive or 'lock-in' amplifier (LIA) which is used to generate a difference signal. The problem described above arises because both the amplitude and wavelength of the laser are modulated by the applied modulation of the laser driving current. The difference signal is therefore not equal to zero at line centre: in practice, therefore, an offset must be applied to the output of the LIA. The size of this offset varies in proportion to the photomultiplier output signal amplitude. Although mirrors are arranged to keep the reference beam stationary as far as possible, small deflections do occur as the laser carriage is moved which cause changes in the photomultiplier output amplitude and therefore in the required offset. The lack of success in constructing a wavelength standard with a sufficiently sharp absorption minimum means that, at present, the best way to find line centre is by watching the absorption signal on the digital storage oscilloscope while slowly tuning the laser back and forth across the transition. This inefficient procedure is probably responsible for the ragged appearance of the points in figure 10.8.

Figure 10.9 seems to show that the most intense part of the discharge is displaced from the geometrical centre. Because there appears to be no mechanism by which this could occur, it is likely that similar wavelength-centering problems have affected the measured absorptions of the first couple of points.

The measured shapes of the concentration distributions are in qualitative agreement with expectations, the greatest concentration occurring near the centre of the discharge volume where the current density is high and the (absorbing) electrodes are distant. Figure 10.8 appears to show a non-zero concentration of metastables at the cathode surface, but this may be due to a background contribution from metastable atoms which are beyond the electrode radius along the line of the beam.

The curves were constructed using the Fourier-Bessel model of chapter 6. The appropriate discharge parameters were taken from Kruithof (1940), Lakshminarasimha

and Lucas (1977) and Kücükarpaci and Lucas (1981). The concentration was first calculated as a function of radius from the axis of the discharge and then Abel-transformed. Because of the seemingly systematic error in the experimental values, the amplitude of the theoretical curves was only approximately adjusted for best fit. The amplitude is, however, the same in both figures.

An estimate was made of the ejection efficiency γ_m by calculating the flux of metastable particles into the cathode and comparing this to a separate measurement of the amplitude of the 'slow' part of the discharge current. The resulting value was 0.85 electrons ejected per metastable-particle impact. A perusal of table 2.2 on page 19 shows that this is a high value, but not an impossible one, particularly for a gas-covered surface.

As mentioned at the start of this section, the excitation coefficient α_m can be calculated if γ_m and the ion amplification factor $S(d)$ are known. $S(d)$ can be measured in the discharge by comparing the 'fast' current $I_{fast}(d)$ with I_0, the limiting value as the electrode separation d approaches the non-equilibrium separation d_0,* provided that the electric field is kept constant as d is varied. The excitation coefficient was calculated to be 0.26 cm^{-1}, which is consistent with the result obtained in the next section (at a slightly higher value of E/N).

Because relatively large values of current were used in this experiment in order to increase the signal-to-noise ratio of the absorption signal, it is important to investigate the possible distortion of the uniform 'vacuum' electric field by the concentrations of charges in the gap. Although the majority of the current is always carried by electrons, the ionic species contribute more to the charge concentration because they drift at a much lower speed than electrons. The electron component is therefore neglected in the following analysis.

The electric field E is obtained by integrating Poisson's equation, which in the present geometry is

$$\frac{d^2V}{dz^2} = -\frac{\rho(z)}{\varepsilon} \qquad (10.2a)$$

* About 0.1 cm at the values of pressure and field under discussion (Kruithof 1940).

where V is the potential, ρ is the charge concentration at distance z from the cathode and ε is the permittivity. The last quantity may be approximated closely by ε_0, the permittivity of the vacuum. The concentration of ions may be found from the methods described in chapter 2, giving

$$\rho(z) = \frac{j(d)}{w}\left[1 - e^{\alpha_i(z-d)}\right] \qquad (10.2b)$$

and thus

$$E = E_0 + \frac{j(d)}{\varepsilon_0 w}\left[z - \frac{1}{\alpha_i}e^{\alpha_i(z-d)}\right], \qquad (10.2c)$$

where E_0 is the vacuum field, $j(d)$ is the current density measured at the anode, d is the electrode separation and α_i is Townsend's primary ionisation coefficient. It is not difficult to show that the maximum departures from the vacuum field occur at $z = 0$ and $z = d$. By using the values of w and α_i appropriate to the value of E_0/N at which the steady-state absorption measurement was made (Hornbeck 1951; Kruithof 1940), and assuming a value of about 10 cm^2 for the average cross-sectional area of the ion current, the maximum field perturbation evaluates to be about 3.6% for 200 nA of anode current. This is regarded as acceptable for this experiment.

10.4. Rates of production of metastable atoms.

It was shown in section 5.4 that the rate of rise of the concentration of metastable particles is proportional to the product of the excitation coefficient and the electron number density, provided the measurement is made after the 'fast' discharge processes involving electrons, ions and excited states of short lifetime have reached a quasi-equilibrium and before significant numbers of metastable atoms have reached the cathode. The existence of such a 'window' of time is demonstrated by the recording of discharge current in figure 10.10. There is a period of about a millisecond in which the fast rise in the current has saturated but the contribution from metastables is not yet significant. Measurements of the rate of rise in the concentration of metastables during this period ought, therefore, to return accurate values for the electron concentration.

Note that the value of the anode current, and therefore the size of the perturbations of the vacuum field due to space charge, is typically an order of magnitude lower in these experiments than those described in the previous section.

Measurements of this rate of rise were performed, along one axial and two radial transects. The results are shown in figures 10.11 and 10.12, which appear on the next page. The Fourier-Bessel model was again used to calculate the theoretical curves, rather than the method of chapter 5, because the necessary computer programs had already been written. Because the concentration of electrons can be seen to drop to negligible levels well within the electrode radius R_E, it seems unlikely that there would be any significant difference between the two models in the present case. Once again, in view of the relatively poor quality of the data, no attempt was made to obtain the best fit between the model curves and the data values. Different amplitudes were used in each figure, although the two curves in figure 10.12 have been given the correct relative sizes.

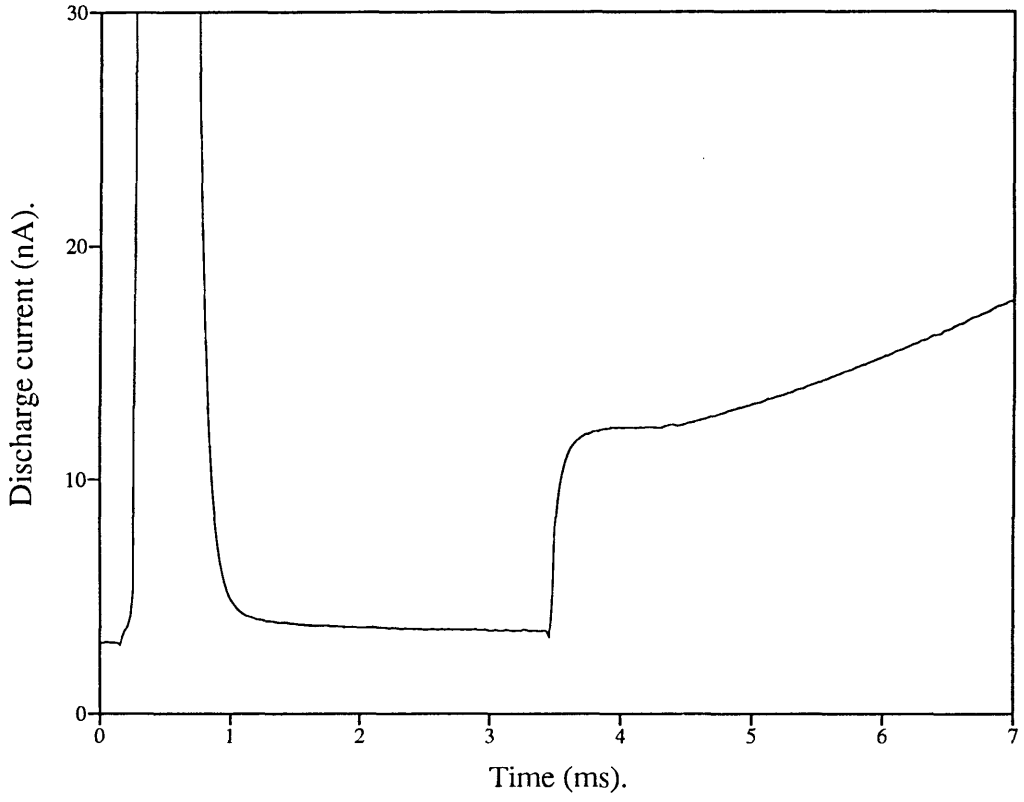

Figure 10.10. An example of the current passed by the discharge during an absorption experiment. The large (truncated) positive-going spike at about 0.5 ms occurs at the time the potential difference is introduced between the electrodes, and represents a displacement current rather than a flow of charged particles through the gas. The true current commences at 3.5 ms when the ultraviolet light is turned on. This shows the familiar form of a sharp rise as the charged particles and short-lived excited states come into equilibrium, followed by a slow rise as metastable particles begin to diffuse to the cathode. The instrumental time constant for this trace was about 0.7 μs.

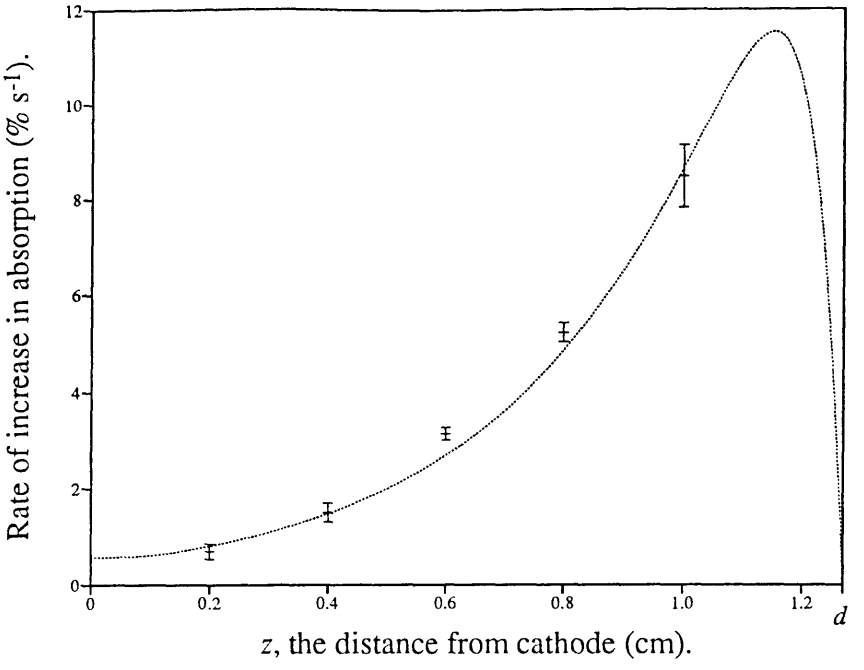

Figure 10.11. The rate of increase in the optical absorption after the commencement of the discharge. The dotted line represents the values returned by the model of chapter 6. The gas number density is the same as that of figures 10.8 and 10.9, but the reduced field is slightly higher at 454 Td.

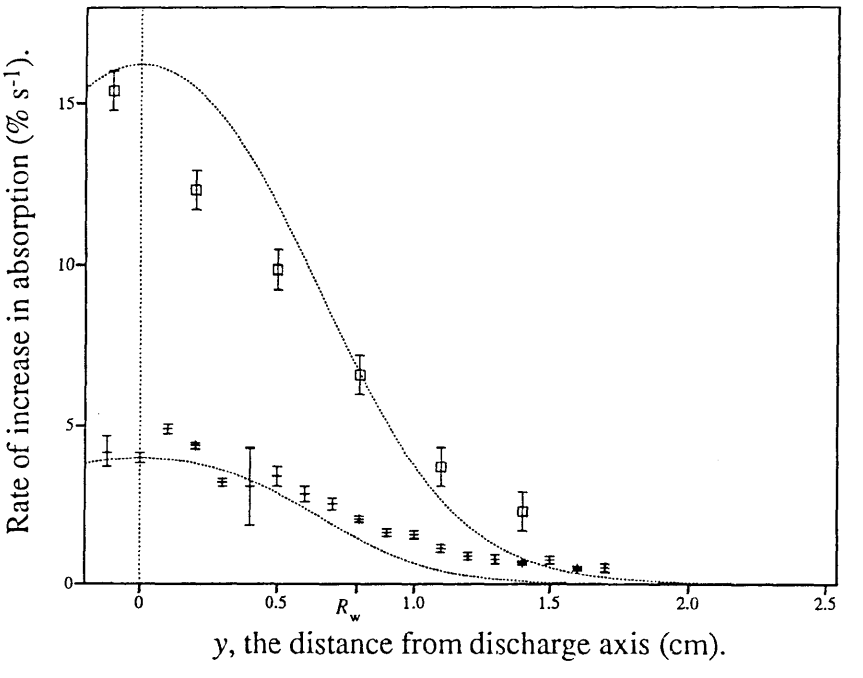

Figure 10.12. The rate of increase in the optical absorption across two radial transects. The crosses and boxes represent, respectively, measurements taken at 0.6 and 1.1 cm from the cathode. The dotted lines are the model predictions. The discharge parameters are identical to those of figure 10.11.

These observations were subject to the same wavelength-centering problems as the steady-state measurements. Also, the uncertainty in fitting a curve to the data was generally higher than before, due partly to the smaller length of trace which was available to analyse. The problem was exacerbated by the fact that the measurements were taken with the voltage switched on and off without a similar modulation of the ultraviolet lamp. The discharge commences at the point at which the voltage is turned on, rather than the instant the lamp radiation appears. The voltage rise time is much slower than the rise time of the lamp and was therefore able to 'smear out' the initial rise in metastable concentration. The scheme in which the lamp is switched on slightly after the voltage supply was not attempted at the start of proceedings, as an overvoltage was being used and it was feared that spontaneous discharges would occur in the period between the voltage and lamp switch-on times. This was later found not to be a problem and, in fact, further reflection shows that it is not likely to be a problem at the voltages and time scales which have been employed. This is because the overvoltage which was used was not so high as to cause a breakdown due to ion-produced secondary electrons; the current run-away occurs only after the full flux of metastable particles begins to reach the cathode. Any electrons that are present in the discharge between the time the voltage is applied and the time at which the lamp is switched on may, therefore, cause an exponential increase in the current and therefore, technically speaking, a 'breakdown', but the amplitude of this current will be very small. This is because this amplitude is given by the product of the ion amplification factor $S(d)$ and the amount of primary current leaving the cathode, which is negligible in the absence of radiation from the ultraviolet lamp. Therefore, so long as the interval between the application of the potential difference and the lamp is not excessive, a 'spontaneous discharge' cannot occur.

The above notwithstanding, the technique is clearly successful at mapping the steady-state electron concentration rather than that of the metastable particles. Note, for example, that the electron distribution predicted by the model is much more strongly peaked near the anode than the metastable-particle distribution. The experimental points follow this shape very well. Also, a generally more compact radial distribution is also exhibited by both the experimental and theoretical electron number densities.

The following deductions can be drawn from these data. The ratio between the areas under the two curves in figure 10.12 is equal to the increase in electron current between d_1 and d_2, the two distances at which the data were taken. From equation (2.1), this is equal to $\exp[\alpha_i(d_2-d_1)]$. The value of α_i can therefore be determined. The result is 2.0 cm^{-1},

which is broadly consistent with the value of 3.1 cm^{-1} recorded by Kruithof (1940) at the same field and pressure. The agreement becomes better when it is considered that diffusion of the electrons is not negligible under the conditions being discussed. Application of equation (2.38) shows that values of α_i determined at this pressure and field by using a Townsend-type experiment are about 15% too large. The correct value is therefore probably nearer to 2.7 cm^{-1}. Agreement becomes even better when the whole of figure 10.11 is considered. The theoretical curve in this figure was calculated using the diffusion-corrected value of 2.7 cm^{-1}; the general fit to the experimental points can be seen to be good.

The excitation coefficient α_m can be calculated from the area under either curve in figure 10.12. This area is equal to

$$\int dx\, \dot{\kappa}(x,z) = \int dx \int dy\, \dot{k}(x,y,z) \tag{10.3}$$

$$= \sigma \int dx \int dy\, \dot{n}_m(x,y,z) \tag{10.4}$$

$$= \sigma \dot{N}_m(z), \tag{10.5}$$

where σ is the optical absorption cross-section. From equations (5.14) and (5.53), this is approximately equivalent to

$$\int dx\, \dot{\kappa}(x,z) = \sigma \alpha_m I(z)/e \tag{10.6}$$

where e is the electronic charge. The value of the excitation coefficient α_m can therefore be deduced. The resulting value of 0.24 cm^{-1} is not very close to the value of 0.9 cm^{-1} reported by Tachibana (1986) at the same field and pressure, although it is consistent with the value reported in section 10.3. Note also that values of this quantity are known with much less certainty than the ionisation coefficient.

11. Conclusion.

In this work, a number of theoretical and experimental studies are described of the pre-breakdown discharge, in argon, between plane-parallel electrodes. Measurements of the current passed by the discharge are discussed as well as measurements of the light absorbed by excited atoms in the discharge. Chapter 2 reviews the Townsend experiment, in which the steady-state current is measured as a function of electrode separation, the electric field being maintained at a constant value. Modifications to the basic Townsend theory to accommodate contributions to the total current by secondary electrons ejected from the cathode by diffusing metastable particles are discussed and the effects of diffusive motions of the electrons are briefly covered.

Time-resolved experiments are discussed in chapter 3. The solution of the homogeneous, time-dependent diffusion equation for metastable particles is reviewed. Conditions at an absorbing boundary are discussed at some length. Many authors have reported that the concentration $n_m(z)$ of metastable particles does not appear to decrease to zero at a boundary, which raises the question of the correct boundary condition to apply when attempting to solve the diffusion equation. It is agreed that the condition at a boundary at $z = 0$ must be of the form

$$n_m(0) - \beta \frac{\partial n_m(0)}{\partial z} = 0, \qquad (11.1)$$

but several different expressions for the boundary coefficient β have been proposed. A new expression is derived in section 3.1.1 which is unique in that β is predicted to be zero at a perfectly absorbing surface. However, this result does not appear to be consistent with measurements of very small values for the fraction of metastable atoms in an atomic beam which are reflected from a surface without being 'quenched' (Conrad *et al* 1982a, b).

Section 3.2 discusses the experiment of Molnar (1951a, b) in which changes in the discharge current are measured as the source of primary current is cycled on and off. Measurements of the time constant of the slow decay of current due to metastable-produced secondaries can be used to determine effective values of the diffusion and volume quenching coefficients. An alternative approach to the analysis of this experiment is described, which has a different set of advantages and disadvantages to Molnar's analysis. The discovery by Ernest (1995a) that complex-valued decay constants may occur

in the slow current waveform is investigated. It is found that these complex decays occur in many gases and over a wide range of discharge conditions. The susceptibility to the occurrence of complex components in the slow-current decay is shown to increase with a decrease in the efficiency of ejection of electrons from the cathode by metastable-particle impact. This seems to be counter-intuitive and may bear further investigation. In a later chapter (chapter 9) it is shown that there are circumstances in which Molnar's analysis returns grossly incorrect values of the free-decay time constants.

Chapter 4 discusses the interaction between laser light and the populations of excited states in the discharge. If it is desired to make spatially-resolved measurements of the concentrations of excited states, a beam of radiation of small radius must be used; also, signal-to-noise considerations prevent the use of very low-powered beams. These two criteria, together with the narrow bandwidth of the light sources used, result in a significant radiant intensity within the beam, which introduces the possibility that a degree of saturation of the absorption coefficient may occur. Considerable attention is therefore paid to the onset of saturation. Several models of the interaction between the light beam and the discharge are examined. Interestingly, it is found that the decrease in the absorption coefficient with intensity follows the same functional form in all situations, the only difference being the intensity of the radiation at the onset of saturation.

The effect of the laser radiation on the rate of decay of metastable particles is investigated in section 4.3. It is shown that the maximum perturbation is about 20%.

Two principal techniques of spatially-resolved measurement of metastable-particle concentrations suggest themselves: measurement of the rate of rise in concentration after the commencement of the discharge, and measurement of the steady-state concentration. Chapters 5 and 6 lay the theoretical foundations for the analysis of these techniques. Chapter 5 treats ways of modelling the distribution of electrons. The hydrodynamic approximation is assumed in which the distribution of electrons is represented by a second-order diffusion equation. Although this approximation becomes poor near the electrodes, it is shown that the desired information can be obtained by measurements made far from these surfaces, and hence that the diffusion equation is a valid approximation from this standpoint. The diffusion equation is solved using the Hankel transform. It is pointed out that this method has advantages when it is necessary to compare theoretical solutions of the electron distribution with the experimental measurements. This is because the experiment yields an Abel transform of the electron concentration function. The

theoretical concentration function, easily found in Hankel space, can be converted from this to an Abel form by the application of a numerical Fourier transform.

In chapter 6, the three-dimensional distribution of metastable particles is addressed. The main intent in this chapter is to enable the secondary ejection efficiency γ_m to be measured with accuracy using a small number of optical absorption measurements. Although the diffusion equation is rigorous in this case, the situation is made more complicated by the fact that the concentration of metastables is causally related to the concentration of electrons, although the reverse is not true. It is shown that the coupled equations can be reduced to a single integral equation which can be solved numerically; alternatively, expansion of the electron concentration in a Fourier-Bessel series allows the coupled differential equations to be reduced to an infinite series of linear equations, which may be truncated and inverted. A third solution method, applicable only in cases where the diffusive motion of the electrons can be ignored, is to replace the differential equation for metastables by a finite-difference approximation. These three solution methods are compared. Overall, the Fourier-Bessel approach seems to be the most useful.

The Fourier-Bessel formalism developed in chapter 6 allows an examination of the effects upon the discharge of a radial variation in the secondary ejection efficiency across the cathode surface. Such a variation had been suspected by Ernest (1991) of causing a peculiar effect in the nitrogen discharge. The model which was developed is very successful at explaining this effect.

Chapters 7 and 8 discuss the experimental arrangements and methods of digitally processing recorded signals. A new (as far as the author knows) method of filtering exponential decays without distortion is presented.

Measurements of the discharge current are reported in chapter 9. The primary ionisation coefficient was measured using the technique of Haydon and Williams (1976), but the expected decrease in the values below those recorded with the whole current was not seen. The raised values were interpreted as evidence that non-negligible levels of impurity were present in the gas samples, either before or after they were admitted to the chamber.

Section 9.2 describes the results of measurements of the Molnar type. The validity of Molnar's analysis was directly investigated and found to be problematical within the

regimes which were investigated. Several peculiar effects are described, and attempts to detect oscillatory decays are reported. Measurements of the diffusion and quenching parameters were made. A higher than expected value for the quenching coefficient was found (no doubt due to the impurity level), but the value of the diffusion coefficient agreed very well with previous measurements. Finally, measurements were made of the breakdown voltage at various pressures and electrode separations.

Chapter 10 describes a variety of optical absorption experiments. First of all, the saturation behaviour of the absorption coefficient was examined. The data were found to follow the predicted shape curve within experimental error, although the value of the saturation power was a factor of 100 larger than the value predicted using the theory of section 4.2.2. No perturbation of the decay rate of the metastable concentration could be detected, although an optogalvanic signal could be seen when the discharge was near to breakdown.

The variation with d of the rate of decay in concentration of the metastables was found to agree well with the predictions of theory, although problems were experienced at low pressure due to a large-amplitude, slowly decaying background component which was caused by an enhanced production of metastables around the longer path between the electrode edges.

A series of measurements of the steady-state concentration of metastable particles were performed. One line of measurements was made along the axis of the discharge (ie, at several values of z for $y = 0$), whereas the other was made across the axis, varying y but keeping z constant. The steady-state distribution of metastables showed the expected 'hump' in the middle of the discharge.

The initial rate of rise in concentration was measured along one axial transect and two radial transects. Measurements of the rise of current confirmed that a 'window' of time existed between the end of the 'fast' processes and a the commencement of a significant contribution to the current from metastable-produced secondaries. The measured shape of the rate-of-rise function was clearly appropriate to electrons rather than metastables. In particular, the axial transect exhibited an exponential rise with z rather than the 'humped' form expected of particles whose motions are entirely diffusive. Values for the ionisation and excitation coefficients were calculated. The ionisation coefficient was broadly consistent with previous values, but the value of the excitation coefficient was about three

times smaller than the value of Tachibana (1986) taken at the same electric field and gas pressure.

In this work, efficient methods of modelling the concentrations of both electrons and metastable excited particles have been developed. Some preliminary absorption measurements have also been performed, which have indicated the potential of the technique to return values of quantities which are difficult to measure with accuracy by other methods. A number of improvements need to be made, however. The laser should be mounted on an optical bench and the scanning done by means of moveable mirrors, or, even better, by moving the discharge chamber itself. Better control of the laser wavelength is essential. An external-cavity arrangement would be of great assistance as it would permit the wavelength of the laser to be modulated while the amplitude is held constant (Fleming and Mooradian 1981, Filimonov and Borysow 1995). (This would also prevent loss of power in side-modes.) Replacement of the monochromator by a system of etalons or a single multi-layer filter would also assist, as would the introduction of a narrow-line wavelength reference. A multi-channel detection scheme, using a CCD camera for example, would also do much to resolve the difficulties of this experiment.

The technique could easily be extended to other gases, such as krypton or nitrogen, which have electronic transitions within the wavelength ranges at which diode lasers are available. Also, higher power diode lasers can be obtained, which might be used to produce a sizeable optogalvanic response in argon. A comparison of the results with the optogalvanic behaviour of neon, in which the 1s levels are much more closely coupled, might be instructive.

Appendix A: Optimum depth of absorption features in a wavelength reference.

It is a common practice in spectroscopy to use atomic or molecular transitions as wavelength reference points. In the present experiment this is most conveniently accomplished by examining the relevant transitions in absorption. The intensity $I(d,\lambda)$ transmitted through an absorbing medium of thickness d is given by the Beer-Lambert law as

$$I(d,\lambda) = I(0)\exp\left[-\bar{k}(\lambda)d\right]. \qquad \text{(A.1)}$$

The averaged absorption coefficient $\bar{k}(\lambda)$ can be expressed as a product of the average absorption at line centre $\bar{k}_0$ and a lineshape function $g(\lambda - \lambda_0)$. The derivative of the absorption lineshape I is detected by the wavelength modulation technique described in chapter 7. The best resolution of $\partial I/\partial\lambda$ at line centre is therefore obtained when the second derivative $\partial^2 I/\partial\lambda^2$, given at line centre by

$$\left.\frac{\partial^2 I}{\partial\lambda^2}\right|_{\lambda=\lambda_0} = -I(0,\lambda_0)\bar{k}_0 d\exp\left(-\bar{k}_0 d\right)\left.\frac{\partial^2 g}{\partial\lambda^2}\right|_{\lambda=\lambda_0,} \qquad \text{(A.2)}$$

reaches its maximum value as a function of $\bar{k}_0 d$, the optical depth at line centre. This occurs when $\bar{k}_0 d = 1$. The optimum line depth is therefore 1-1/e, or about 63%.

Appendix B: The curve fitting program.

Many of the experiments described in this thesis returned data in the form of an infinite sum of exponentials. In order to analyse these experiments it was found necessary to obtain the amplitudes and decay constants of several of the early terms of such a sum; in practice, no more than two terms were ever required. A computer program was written by the author to fit to such experimental data a function of the form

$$f(\mathbf{p},k) = p_0 + p_1 \exp\left[-(k-k_0)/p_2\right] + p_3 \exp\left[-(k-k_0)/p_4\right]. \quad \text{(B.1)}$$

The quantity k in this expression is the channel number of the data sample.

A generalised function $f(\mathbf{p},k)$ may be fitted to a set of data values d_k between channels a and b by finding the set of parameters $\mathbf{p}_0$ that minimises the sum of squared residuals R, defined by

$$R(\mathbf{p}) = \sum_{k=a}^{b} r_k^2 \quad \text{(B.2)}$$

where

$$r_k = f(\mathbf{p},k) - d_k. \quad \text{(B.3)}$$

Expanding R about $\mathbf{p}_0$ gives

$$R(\mathbf{p}) = R(\mathbf{p}_0) + \tfrac{1}{2}(\mathbf{p}-\mathbf{p}_0)^{\mathrm{T}} \mathbf{C}_{\mathbf{p}_0} (\mathbf{p}-\mathbf{p}_0) + \mathrm{O}(p^3). \quad \text{(B.4)}$$

The first order term has been omitted because it is equal to zero at $\mathbf{p} = \mathbf{p}_0$. The elements of the curvature matrix $\mathbf{C}_{\mathbf{p}_0}$ are given by

$$C_{ij} = \left.\frac{\partial^2 R}{\partial p_i \partial p_j}\right|_{\mathbf{p}=\mathbf{p}_0}; \quad \text{(B.5)}$$

by use of equations (B.2) and (B.3) this can be shown to evaluate to

$$C_{ij} = 2\sum_{k=a}^{b}\left(\frac{\partial f_k}{\partial p_i}\frac{\partial f_k}{\partial p_j}\right)\Bigg|_{\mathbf{p}=\mathbf{p}_0} + 2\sum_{k=a}^{b}\left[f(\mathbf{p}_0,k) - d_k\right]\frac{\partial^2 f_k}{\partial p_i^2}\Bigg|_{\mathbf{p}=\mathbf{p}_0}. \quad \text{(B.6)}$$

If the function $f(\mathbf{p}_0,k)$ is a good fit to the experimental data then the second sum is

$$2\sum_{k=a}^{b} n_k \left.\frac{\partial^2 f_k}{\partial p_i^2}\right|_{\mathbf{p}=\mathbf{p}_0}, \tag{B.7}$$

where n_k represents the random noise that is unavoidably present in the experimental data. If f is a slowly varying function of k, this sum may be neglected. If the first sum in equation (B.6) is approximated by an integral, we arrive at a final expression for the elements of $\mathbf{C}_{\mathbf{p}_0}$:

$$C_{ij} \approx 2\int_a^b dk \left.\left(\frac{\partial f_k}{\partial p_i}\frac{\partial f_k}{\partial p_j}\right)\right|_{\mathbf{p}=\mathbf{p}_0}. \tag{B.8}$$

This expression permits the evaluation of closed-form expressions for the elements of $\mathbf{C}_{\mathbf{p}_0}$. This usually results in a considerable saving in computing time.

The minimum in $R(\mathbf{p})$ can be found by using a variation of Newton's method (Bevington 1969) whereby the vector $\mathbf{p}$ - $\mathbf{p}_0$ is approximated by inverting the expression

$$\nabla R_{\mathbf{p}} \approx \mathbf{C}_{\mathbf{p}}(\mathbf{p}-\mathbf{p}_0) \tag{B.9}$$

where the $\mathbf{p}$ subscripts indicate that ∇R and $\mathbf{C}$ are evaluated at $\mathbf{p}$ rather than (the as yet unknown) $\mathbf{p}_0$. In the computer program, the gradient ∇R was approximated by use of the simple finite difference formula

$$\frac{\partial R}{\partial p_i} \approx \frac{R(\mathbf{p}+\Delta p_i)-R(\mathbf{p}-\Delta p_i)}{2\Delta p_i}. \tag{B.10}$$

Equation (B.9) was inverted using an LU factorisation method (Fisher 1988). The curvature matrix and gradient vector were then re-evaluated at the new set of p values. This procedure was repeated until the fitting routine was judged to have converged. The 'goodness of fit' can be assessed by calculating the parameter χ^2, defined (for a function having m free parameters) by

$$\chi_n^2 = \frac{R_n}{(b-a-m+1)\sigma^2} \tag{B.11}$$

where R_n is the value of R after the nth iteration and the variance σ^2 is given by

$$\sigma^2 = \frac{1}{b-a+1}\sum_{k=a}^{b} n_k^2. \qquad \text{(B.12)}$$

The fitting routine was judged to have converged when the decrease in χ^2 with each iteration fell below some previously specified value.

It is necessary to pay some attention to the choice of Δp_i in equation (B.10): too small a value will produce an inaccurate approximation to ∇R due to truncation errors during the computation; too large a value may invite the same problem due to anharmonic terms in the expansion of R. Treating R and f for simplicity as functions of $x = p_i$, equation (B.10) becomes

$$R'(x) \approx \frac{R(x+\Delta x) - R(x-\Delta x)}{2\Delta x}. \qquad \text{(B.13)}$$

The statistical uncertainty $\sigma_{R'}$ in this calculation can be shown to be approximately equal to $\sigma_R/\Delta x$. The uncertainty in R can be calculated using equations (B.2) and (B.3), giving

$$\sigma_R^2 = \sigma_{\text{trunc.}}^2 + 4\sum_{k=a}^{b} r_k^2 \sigma_k^2 \qquad \text{(B.14)}$$

where

$$\sigma_k^2 = \sigma_{f_k}^2 + \sigma_{d_k}^2. \qquad \text{(B.15)}$$

Since R was calculated to double precision, the truncation error σ_{trunc} is given by

$$\sigma_{\text{trunc.}} \approx 5\times10^{-16} R. \qquad \text{(B.16)}$$

The data values were digitised measurements of voltage, usually to 16 bit precision; data as received from the DSO were therefore integers in the range -32768 to 32767. These were multiplied by a conversion factor A to reproduce the original voltages; hence

$$d_k = A t_k, \qquad \text{(B.17)}$$

where t_k represents the raw integer-valued data. Consequently

$$\sigma_{d_k}^2 = t_k^2 \sigma_A^2 + A^2 \sigma_{t_k}^2 \qquad \text{(B.18)}$$

and thus

$$\sigma_k^2 = \sigma_{f_k}^2 + t_k^2\sigma_A^2 + A^2. \tag{B.19}$$

Note that $\sigma_{t_k}^2 = 1$ has been applied in the last expression. Since A and f_k are both stored as single-precision floating point numbers, we have

$$\sigma_A \approx 5\times10^{-8}A \tag{B.20}$$

and

$$\sigma_{f_k} \approx 5\times10^{-8}f_k. \tag{B.21}$$

Equation (B.19) can therefore be written as

$$\sigma_k^2 = \left(f_k^2 + d_k^2\right)\times2.5\times10^{-15} + A^2. \tag{B.22}$$

Since $f_k \sim d_k = At_k$, the end result is

$$\sigma_k^2 \approx A^2\left(5\times10^{-15}t_k^2 + 1\right), \tag{B.23}$$

or rather

$$\sigma_k \approx A, \tag{B.24}$$

because t_k^2 must be less than 2^{32} (about 10^9). Substitution of equations (B.24) and (B.16) into (B.14) produces

$$\sigma_R^2 = 2.5\times10^{-31}R^2 + 4A^2R. \tag{B.25}$$

Now, the largest possible value of R occurs in the case that b - a = 4096 (the total number of channels used in the program) and $r_k = 2^{16}A\ \forall\ k$. In other words,

$$R < 1.76\times10^{13}A^2. \tag{B.26}$$

This implies that

$$4A^2R > 2.2\times10^{-13}R^2. \tag{B.27}$$

The second term in equation (B.25) can therefore be seen to be completely dominant. To a good approximation, then, the statistical uncertainty in the finite difference expression (B.13) is given by

$$\sigma_{R'} \approx \frac{2A\sqrt{R}}{\Delta x}. \tag{B.28}$$

The systematic error in equation (B.13) may be found by expanding R in terms of x:

$$R(x+\Delta x) = R(x) + \Delta x R'(x) + \frac{(\Delta x)^2}{2} R''(x) + \frac{(\Delta x)^3}{6} R'''(x) + O\left[(\Delta x)^4\right]. \tag{B.29}$$

The finite difference approximation to the first derivative therefore actually gives

$$\frac{R(x+\Delta x) - R(x-\Delta x)}{2\Delta x} = R'(x) + \frac{(\Delta x)^2}{6} R'''(x) + O\left[(\Delta x)^4\right]. \tag{B.30}$$

A little calculus shows that the total uncertainty in R' is minimised when

$$(\Delta x)^3 = \left| \frac{6A\sqrt{2R}}{R'''} \right|. \tag{B.31}$$

Note that, in the case that f is described by equation (B.1), R is purely quadratic in the p_0, p_1 and p_3 directions; the third and higher derivatives therefore do not exist. In this case an appropriate value for Δx can be found by equating the statistical uncertainty given by equation (B.28) with the truncation error in the (single-precision) number R'.

Bibliography

Abdulla R R, Dutton J and Williams A W (1979) *J. Phys. Colloq. C* **7** 73-4

Abramowitz M and Stegun I A (editors) (1972) *Handbook of Mathematical Functions* (New York: Dover)

Amies B W and Fletcher J (1983) *J. Phys. D: Appl. Phys.* **16** L133-6

Barbet A, Sadeghi N and Pebay-Peyroula J C (1975) *J. Phys. B: Atom. Molec. Phys.* **8** 1776-84

Benjamin P and Weaver C (1961) *Proc. Royal Soc. London A* **254** 516-31

Bennett W R Jr. (1961) *Phys. Rev.* **126** 580-93

Berglund C N and Spicer W E (1964) *Phys. Rev.* **136 A** 1044-64

Bertolini G, Bettoni M and Bisi A (1953) *Phys. Rev.* **92** 1586

Bevington P R (1969) *Data Reduction and Error Analysis for the Physical Sciences* (New York: McGraw-Hill)

Beyer W and Haberland H (1984) *Phys. Rev. A* **29** 2280-2

Bhattacharya A K (1976) *Phys. Rev. A* **13** 1219-25

Birot A, Brunet H, Galy J, Millet P and Teyssier J L (1975) *J. Chem. Phys.* **63** 1496-03

Blevin H A and Fletcher J (1984) *Aust. J. Phys.* **37** 593-600

Blevin H A and Fletcher J (1992) *Aust. J. Phys.* **45** 375-86

Blevin H A, Fletcher J, Hunter S R and Marzec L M (1976a) *J. Phys. D: Appl. Phys.* **9** 471-9

Blevin H A, Fletcher J and Hunter S R (1976b) *J. Phys. D: Appl. Phys.* **9** 1671-9

Blevin H A, Fletcher J and Hunter S R (1978) *J. Phys. D: Appl. Phys.* **11** 2295-303

Borst W L (1971) *Rev. Sci. Instrum.* **42** 1543-4

Bouciqué R and Mortier P (1970) *J. Phys. D: Appl. Phys.* **3** 1905-11

Bracewell R (1965) *The Fourier Transform and its Applications* (New York: McGraw-Hill), chapter 12

Bréchignac C, Vetter R and Berman P R (1977) *J. Phys. B: Atom. Molec. Phys.* **10** 3443-50

Bréchignac C, Vetter R and Berman P R (1978) *Phys. Rev. A* **17** 1609-13

Brunker S A K (1984) *Ph. D. Thesis* (University of New England, Armidale)

Brutschy B and Haberland H (1979) *Phys. Rev. A* **19** 2232-48

Burgmans A L J and Smeets A H M (1983) *J. Phys. D: Appl. Phys.* **16** 755-62

Buursen C G J, De Hoog F J and Van Montfort L H (1972) *Physica* **60** 244-56

Chapman S and Cowling T G (1970) *The Mathematical Theory of Non-uniform Gases* 3rd edition (Cambridge University Press), chapter 6

Clark A M, Din F, Robb J, Michels A, Wassenaar T and Zwietering T (1951) *Physica* **17** 876-84

Colli L and Facchini U (1954) *Phys. Rev.* **96** 1-4

Conrad H, Doyen G, Ertl G, Küppers J, Sesselmann W and Haberland H (1982a) *Chem. Phys. Lett.* **88** 281-5

Conrad H, Ertl G, Küppers J, Sesselmann W, Woratschek B and Haberland H (1982b) *Surf. Sci.* **117** 98-108

Cooley J W and Tukey J W (1965) *Math. Comput.* **19** 297-301

Copley G H and Lee C S (1975) *Can. J. Phys.* **53** 1705-14

Cordover R H and Bonczyk P A (1969) *Phys. Rev.* **188** 696-700

Crompton R W (1967) *J. Appl. Phys.* **38** 4093-4

Dall'Armi G, Brown K L, Purdie P H and Fletcher J (1992) *Aust. J. Phys.* **45** 185-91

Davidson P M (1959) *Proc. R. Soc. A* **249** 237-47

Davies D E and Milne J G C (1959) *Brit. J. Appl. Phys.* **10** 301-6

Dielis J W H, de Hoog F J and Schram D C (1979) *J. Phys. Colloq. C* **7** 75-6

Dugdale J S (1977) *The Electrical Properties of Metals and Alloys* (London: Edward Arnold), chapter 12

Dunning F B, Smith A C H and Stebbings R F (1971) *J. Phys. B: Atom. Molec. Phys.* **4** 1683-95

Dunning F B and Smith A C H (1971) *J. Phys. B: Atom. Molec. Phys.* **4** 1696-1710

Dutton J (1975) *J. Phys. Chem. Ref. Data* **4** 577-856

Dutton J (1981) *Prebreakdown Ionisation in Gases* in *Electrical Breakdown and Discharges in Gases*, ed. Kunhardt E E and Luessen L H (London: Plenum)

Ellis E and Twiddy N D (1969) *J. Phys. B: Atom. Molec. Phys.* **2** 1366-77

Engstrom R W and Huxford W S (1940) *Phys. Rev.* **58** 67-77

Ernest A D (1991) *Ph. D. Thesis* (University of New England, Armidale)

Ernest A D, Haydon S C and Wang Y (1992) *J. Phys. D: Appl. Phys.* **25** 1187-96

Ernest A D, Haydon S C Fewell M P and Noy M J (1994) *J. Phys. D: Appl. Phys.* **27** 2531-8

Ernest A D (1995a) *J. Phys. D: Appl. Phys.* **28** 1335-45

Ernest A D (1995b), personal communication.

Feron P, Ferales F, Decomps B, Robert J, Reinhardt J, Baudon J and Haberland H (1989) *Chem. Phys. Lett.* **160** 555-8

Filimonov S and Borysow J (1995) *Appl. Opt.* **34** 438-43

Fisher M E (1988) *Introductory Numerical Methods with the NAG Software Library* (Department of Mathematics, University of Western Australia)

Fleming M W and Mooradian A (1981) *IEEE J. Quant. Electron.* **17** 44-59
Fletcher J and Reid I D (1980) *J. Phys. D: Appl. Phys.* **13** 2275-83
Folkard M A and Haydon S C (1971a) *Aust. J. Phys.* **24** 519-26
Folkard M A and Haydon S C (1971b) *Aust. J. Phys.* **24** 527-42
Futch A H and Grant F A (1956) *Phys. Rev.* **104** 356-61
Gardner D G, Gardner J C, Laush G and Meinke W W (1959) *J. Chem. Phys.* **31** 978-86
Golde M F, Ho G H, Tao W and Thomas J M (1989) *J. Phys. Chem.* **93** 1112-8
Gosseries A (1939) *Physica* **6** 458-72
Greene D (1950) *Proc. Phys. Soc. London* **63** 876-89
Greenstein H (1972) *J. Appl. Phys.* **43** 1732-50
Gyorffy B L, Borenstein M and Lamb W E Jr. (1968) *Phys. Rev.* **169** 340-59
Hagstrum H D (1956a) *Phys. Rev.* **104** 672-83
Hagstrum H D (1956b) *Phys. Rev.* **104** 1516-27
Hagstrum H D (1961) *Phys. Rev.* **123** 758-65
Haydon S C, Fewell M P, Ernest A D and Baldwin M J (1995), unpublished.
Haydon S C and Williams O M (1973a) *J. Phys. B: Atom. Molec. Phys.* **6** 1856-65
Haydon S C and Williams O M (1973b) *J. Phys. B: Atom. Molec. Phys.* **6** 1866-80
Haydon S C and Williams O M (1976) *J. Phys. D: Appl. Phys.* **9** 523-36
Heylen A E D (1968a) *Brit. J. Appl. Phys.* **1** 179-88
Heylen A E D (1968b) *Int. J. Electron.* **24** 165-75
Hitchcock A J M (1957) *Math. Tab. Aids Comp.* **11** 86-8
Holstein T (1947) *Phys. Rev.* **72** 1212-33
Holst G and Oosterhuis E (1923) *Phil. Mag.* **46** 1117-22
Hornbeck J A (1951) *Phys. Rev.* **84** 615-20
Hurst C A and Liley B S (1965) *Aust. J. Phys.* **18** 521-40
Huxley L G H (1959) *Aust. J. Phys.* **12** 171-83
Huxley L G H (1972) *Aust. J. Phys.* **25** 523-7
Huxley L G H and Crompton R W (1974) *The Diffusion and Drift of Electrons in Gases* (New York: Wiley)
Jacobs H and LaRocque A P (1946) *J. Appl. Phys.* **18** 199-203
Jacques L, Bruynooghe W, Bouciqué R and Wieme W (1986) *J. Phys. D: Appl. Phys.* **19** 1731-9
Keil R, Schabert A and Toschek P (1973) *Z. Phys.* **261** 71-84
Kenty C (1933) *Phys. Rev.* **44** 891-7
Kolts J H and Setser D W (1978) *J. Chem. Phys.* **68** 4848-59
Kruithof A A and Penning F M (1936) *Physica* **3** 515-33

Kruithof A A and Penning F M (1937) *Physica* **4** 430-49
Kruithof A A (1940) *Physica* **7** 519-40
Kücükarpaci H N and Lucas J (1981) *J. Phys. D: Appl. Phys.* **14** 2001-14
Kumar K, Skullerud H R and Robson R E (1980) *Aust. J. Phys.* **33** 343-448
Lakshminarasimha C S and Lucas J (1977) *J. Phys. D: Appl. Phys.* **10** 313-21
Lamb W E Jr. (1964) *Phys. Rev.* **134 A** 1429-50
Langevin P (1905) *Ann. Chim. Phys.* (8) **5** 245-288
Lawrence G M (1968) *Phys. Rev.* **175** 40-4
Levron D and Phelps A V (1978) *J. Chem. Phys.* **69** 2260-2
Lisitsyn V N, Provorev A S and Chebotaev V P (1970) *Opt. Spectrosc.* **29** 119-22
Lowke J J, Parker J H Jr. and Hall C A (1977) *Phys. Rev. A* **15** 1237-45
Lucas J (1964) *Int. J. Electron.* **17** 43-8
Lucas J (1965) *Int. J. Electron.* **18** 419-30
Luke Y L (1962a) *Integrals of Bessel Functions* (New York: McGraw-Hill), chapter 2
Luke Y L (1962b) *Integrals of Bessel Functions* (New York: McGraw-Hill), chapter 12
Manzanares E R and Firestone R F (1983) *J. Chem. Phys.* **79** 1678-83
Martin P J, Sainty W G, Netterfield R P and Buckley A N (1985) *Vacuum* **35** 621-4
Masters J I (1955) *J. Chem. Phys.* **23** 1865-74
Mattox D M (1966) *J. Appl. Phys.* **37** 3613-5
McCoubrey A O (1954) *Phys. Rev.* **93** 1249-60
McDaniel E W (1964a) *Collision Phenomena in Ionized Gases* (New York: Wiley), chapter 2
McDaniel E W (1964b) *Collision Phenomena in Ionized Gases* (New York: Wiley), chapter 10
Meek J M and Craggs J D (1953) *Electrical Breakdown of Gases* (Oxford: Clarendon), chapter 2
Melton C E, Hurst G S and Bortner T E (1954) *Phys. Rev.* **96** 643-5
Millet P, Barrie A M, Birot A, Brunet H, Dijols H, Galy J and Salamero Y (1981) *J. Phys. B: Atom. Molec. Phys.* **14** 459-72
Molnar J D (1951a) *Phys. Rev.* **83** 933-40
Molnar J D (1951b) *Phys. Rev.* **83** 940-52
Moore D G and Thornton H R (1959) *J. Res. Nat. Bur. Stds.* **62** 127-35
Moore W S and Yalcin T (1973) *J. Mag. Res.* **11** 50-57
Moutard P, Laporte P, Subtil J-L, Damany N and Damany H (1987) *J. Chem. Phys.* **87** 4576-88
Nakamura Y (1987) *J. Phys. D: Appl. Phys.* **20** 933-8

Nakamura Y and Kurachi M (1988) *J. Phys. D: Appl. Phys.* **21** 718-23
Newton R R (1948) *Phys. Rev.* **73** 570-83
Nguyen T D and Sadeghi N (1978) *Phys. Rev. A* **18** 1388-95
Okoshi T, Kikuchi K and Nakayama A (1980) *Electron. Lett.* **16** 630-1
Otieno A V (1978) *Opt. Comm.* **26** 207-10
Parker J H Jr. (1954) *Phys. Rev.* **93** 1148-56
Penning F M and Addink C C J (1934) *Physica* **1** 1007-44
Peters G and Wilkinson J H (1979) *SIAM Rev.* **21** 339-60
Phelps A V and Molnar J D (1953) *Phys. Rev.* **89** 1202-8
Phelps A V (1959) *Phys. Rev.* **114** 1011-25
Provencher S W (1976) *Biophys. J.* **16** 27-41
Ramsauer C and Kolluth R (1929) *Ann. der Phys. V* **3** 536-64
Sadeghi N and Pebay-Peyroula J C (1974) *J. Physique* **35** 353-60
Saelee H T, Lucas J and Limbeek J W (1977) *Solid State Electron. Dev.* **1** 111
Saito S and Yamamoto Y (1981) *Electron. Lett.* **17** 325-7
Schafer R W, Mersereau R M and Richards M A (1981) *Proc. IEEE* **69** 432-50
Schohl S, Meijer H A J, Ruf M-W and Hotop H (1992) *Meas. Sci. Technol.* **3** 544-51
Shirley J H (1973) *Phys. Rev. A* **8** 347-68
Siegman A E (1977) *Opt. Lett.* **1** 13-15
Siegman A E (1986) *Lasers* (California: University Science Books), chapter 3
Shumaker J B and Popenoe C H (1967) *J. Opt. Soc. Am.* **57** 8-10
Skullerud H R (1974) *Aust. J. Phys.* **27** 195-209
Small-Warren N E and Lue-Yung C C (1975) *Phys. Rev. A.* **11** 1777-83
Smith G D (1974) *Numerical Solution of Partial Differential Equations* (Oxford University Press)
Smith M R and Buckmaster H A (1975) *J. Mag. Res.* **17** 29-33
Smith M R and Cohn-Sfetcu S (1975) *J. Phys. E: Sci. Instrum.* **8** 515-22
Smith M R, Cohn-Sfetcu S and Buckmaster H A (1976) *Technometrics* **18** 467-82
Smith P W and Hänsch T (1971) *Phys. Rev. Lett.* **26** 740-3
Sneddon I H (1972) *The Use of Integral Transforms* (New York: McGraw-Hill), chapter 5
Suzuki S, Itoh H, Ikuta N and Sekizawa H (1992) *J. Phys. D: Appl. Phys.* **25** 1568-73
Szöke A and Javan A (1963) *Phys. Rev. Lett.* **10** 521-4
Tachibana K (1986) *Phys. Rev. A* **34** 1007-15
Tachibana K (1991), personal communication.
Tachibana K, Harima H and Urano Y (1982) *J. Phys. B: Atom. Molec. Phys.* **15** 3169-78

Tachibana K and Phelps A V (1987) *Phys. Rev. A* **36** 999-1007

Takakura T, Iga K and Tako T (1980) *Jap. J. Appl. Phys.* **19** L725-7

Tao W, Golde M F, Ho G H and Moyle A M (1987) *J. Chem. Phys.* **87** 1045-53

Thomas J M, Kaufman F and Golde M F (1987) *J. Chem. Phys.* **86** 6885-92

Thonnard N and Hurst G S (1972) *Phys. Rev. A* **5** 1110-21

Townsend J S (1902) *Phil. Mag.* **3** 557-76

Townsend J S and Bailey V A (1922) *Phil. Mag.* **44** 1033-52

Tsurugida K and Ikuta N (1993) *J. Phys. Soc. Japan* **62** 948-58

Vallee O, Ranson P and Chapelle J (1977) *J. Quant. Spectrosc. Radiat. Transfer* **18** 327-36

Varney R N (1954) *Phys. Rev.* **93** 1156-60

Vehse R C and Arakawa E T (1969) *Phys. Rev.* **180** 695-700

Velazco J E, Kolts J H and Setser D W (1978) *J. Chem. Phys.* **69** 4357-73

Virr L E, Lucas J and Kontoleon N (1972) *J. Phys. D: Appl. Phys.* **5** 542-54

Wagner E B, Davis F J and Hurst G S (1967) *J. Chem. Phys.* **47** 3138-47

Wainfan N, Walker W C and Weissler G L (1953) *J. Appl. Phys.* **24** 1318-21

Walker W C, Wainfan N and Weissler G L (1955) *J. Appl. Phys.* **26** 1366-71

Wedding A B, Blevin H A and Fletcher J (1985) *J. Phys. D: Appl. Phys.* **18** 2361-73

Wieman C E and Hollberg L (1991) *Rev. Sci. Instrum.* **62** 1-20

Wieme W and Lenaerts J (1980) *Physica C* **98** 229-34

Wieme W and Lenaerts J (1981) *J. Chem. Phys.* **74** 483-93

Wieme W and Wieme-Lenaerts J (1974) *Phys. Lett. A* **47** 37-8

Wiese W L, Brault J W, Danzmann K, Helbig V and Kock M (1989) *Phys. Rev. A* **39** 2461-71

Weisberg S (1980) *Applied Linear Regression* (New York: Wiley), chapter 4

Yariv A (1976) *Introduction to Optical Electronics* (California: Holt, Rhinehart and Winston), chapter 5